FlatChem 56 (2026) 101017

Contents lists available at ScienceDirect

FlatChem

journal homepage: www.sciencedirect.com/journal/flatchem

Understanding structure-property relationships in graphene oxide-coated polymer membranes: The impact of flake size on dye and salt rejection

James M. Exley [a,*], Timothy N. Hunter [b,*], Fan Fei [c], Thomas Pugh [c,d], Martin R. Tillotson [a,*]

[a] School of Civil Engineering, University of Leeds, Leeds, West Yorkshire LS2 9JT, United Kingdom
[b] School of Chemical and Process Engineering, University of Leeds, Leeds, West Yorkshire LS2 9JT, United Kingdom
[c] Evove, Sci-Tech Daresbury, Keckwick Lane, Daresbury WA4 4AB, United Kingdom
[d] University of Liverpool, 3rd floor, Linear Wing, The Foundation Building, Brownlow Hill, Liverpool L69 7ZX, United Kingdom

ARTICLE INFO

Keywords:
Graphene oxide
Composite membrane
Dye filtration
Desalination
Wastewater treatment

ABSTRACT

Graphene oxide (GO) membranes were fabricated using vacuum filtration and their performance in the removal of dye and salts from effluent was investigated. GO flake size is thought to influence the performance of composite membrane systems. Using smaller flake GO (SFGO) and larger flake GO (LFGO) systems, filtration studies demonstrated that both cationic Methylene Blue (MB) and anionic Methyl Orange (MO) could be effectively removed from water effectively using both systems. The highest removal rates of both dyes were achieved by the 0.10 mg/mL SFGO coating, rejecting 86.4% MB and 87.8% MO, at 2 bar with 5 mg/L dyes. For both GOs, the removal of MO was higher overall, which was attributed to electrostatic repulsion between the like-charged GO and dye. MB was found to adsorb strongly onto the GO coating. Desalination of NaCl, Na_2SO_4, $MgSO_4$ and $(NH_4)_6Mo_7O_{24}$ was found moderately successful, with performance degrading significantly with permeated volume. This behaviour was attributed to the Donnan Effect and expansion of GO interlayer spacing, due to the intercalation of water molecules. The presence of Na_2SO_4 and $MgSO_4$ in MB was demonstrated to degrade both flux and dye rejection capability of both GOs, due to the neutralisation of the electronegativity driven by the salt cations.

1. Introduction

Polymeric membrane systems are becoming a prominent means of removing contaminant species from water, offering simplified processing routes to treat wastewaters containing organic dyes and salts. Similarly, reverse osmosis (RO) membranes are widely utilised in water scarce regions due to their effective desalination capabilities, however, they are limited in operation by their tendency to foul, a hindrance that reduces the permeate flux of cleaned water through the membrane channels [1,2] and increases energy demand [3,4]. Despite continued advancements in pumping and membrane efficiencies, RO membrane systems remain highly energy-intensive [5,6]. Accordingly, these limitations have led to the search for alternative membrane systems with improved operational longevity, permeate flux and fouling resistance.

The nanomaterial graphene oxide (GO) has attracted much attention due to the unique interaction pathways between GO, water and contaminant species, in which its oxygen-containing functionality, resulting in negative surface potential at neutral pH [7], enabling application as both a membrane fabrication [8–10] and as an adsorbent [11–13]. The unique combination of the sp^2 carbon network of the graphene basal plane with the oxygen-containing functional groups renders GO an amphiphilic material [14]. Accordingly, water molecules may slide rapidly through the resulting hydrophilic "gates" while effectively sieving out charged species. Based on their charge characteristics, amphiphilic nature and heterogeneous, oxygen-rich surface chemistry, GO membranes are uniquely positioned as promising candidates for overcoming the operational challenges of existing polymeric membrane systems.

Vacuum filtration is a popular and versatile technique commonly utilised in the fabrication of GO-coated membranes. Typically, a GO suspension is filtered through a porous substrate under applied vacuum conditions [15,16]. Given the large lateral sizes of the GO flakes relative to the substrate pores, the GO flakes accumulate and stack on the membrane surface resulting in a deposited GO coating layer [17]. By varying the dispersed GO concentration, membrane coatings of various thickness ranging from single nm [18] up to tens of microns [19] are

* Corresponding authors.
E-mail addresses: jamesexley2612@gmail.com (J.M. Exley), t.n.hunter@leeds.ac.uk (T.N. Hunter), M.R.Tillotson@leeds.ac.uk (M.R. Tillotson).

https://doi.org/10.1016/j.flatc.2026.101017
Received 25 November 2025; Received in revised form 9 February 2026; Accepted 26 February 2026
Available online 27 February 2026

readily available. Despite its advantages, vacuum filtration is limited to small membrane areas only (a few cm^2 in size), and variations in vacuum pressure can lead to uneven coating thickness [15,20].

GO membranes have demonstrated enhanced separation performance of dye species compared to pristine polymer membranes. For example, Elessawy et al. [21] utilised a vacuum filtration technique to deposit GO onto a polyethersulfone (PES) substrate that could reject methylene blue dye with overall 91% removal efficacy. The mechanism of dye rejection was strongly governed by electrostatic interactions between the GO and the contaminant. For cationic dyes, electrostatic attraction of positively charged molecules to the negatively charged GO surface, followed by subsequent adsorption is the dominant mechanism of separation [22]. Excessive adsorption may however lead to a decline in performance due to fouling of the membrane surface [23,24]. For anionic dye species, adsorption is less significant overall, but electrostatic repulsion between dye and GO is the dominating characteristic, enabling, in some cases, very high dye rejection [22,25–27].

GO membranes are also of key interest as potential alternatives to conventional RO systems for desalination applications [28–30]. In practical operation, however, many studies have achieved only moderate success in removing ionic species from water, which has mainly been attributed to the structural instability of the coating layers during filtration [24,31,32]. GO tends to take up water when hydrated, resulting in expansion of the interlayer spacing since the structure is only held together by weak van der Waals forces and hydrogen bonds [33], leading ultimately to delamination of the layer stack [34]. Interlayer spacings of GO layers of up to 1.3 nm have been reported, resulting in enlarged ionic transport pathways [35]. This structural expansion is widely associated with a decline in the desalting capability of a GO membrane during its run cycle [36–38].

An important parameter governing the structure and transport phenomena of GO membranes is the flake size of the material. Several studies have shown that the solvent permeance through stacked GO membranes is inversely related to the lateral flake size due to shorter transport pathways [39–42]. Conversely, GO membranes fabricated from larger flake dispersions tend to offer higher solute rejection, due to more ordered stacking and fewer structural defects [43]. To illustrate this, Sun et al. [44] considered the performance of stacked GO sheets consisting of nano- and micron-sized flakes, finding that only the latter was capable of rejecting cationic species.

In a previous article [45], the present authors investigated the influence of GO flake size on adsorption of dye molecules from water, employing two commercially available GO materials. Particle sizing techniques demonstrated that the GO materials were of different size distributions, accordingly they were termed smaller flake GO (SFGO) and larger flake GO (LFGO). It was shown that both SFGO and LFGO had a very strong tendency to adsorb cationic Methylene Blue (MB) dye, while the adsorption of anionic Methyl Orange (MO) was, although still promising, lower due to electrostatic interactions between the adsorbent and adsorbate. Furthermore, the prior dissolution of ions into MB reduced the adsorption capacity of the GOs due to charge screening effects. These findings highlight that flake size is an integral feature governing the interaction of GO with contaminants, and motivates a systematic investigation of its impact on membrane architecture and separation performance.

Although previous studies have highlighted the effectiveness of GO membranes for dye and ion separation, few studies have investigated the physicochemical and structural characteristics of commercially sourced GO materials. In order to elucidate how flake size governs membrane architecture, transport phenomena and separation mechanisms, a systematic investigation of flake size-dependent structure-property relationships therefore remains essential in developing a detailed mechanistic understanding of GO-contaminant interactions; this is a key factor governing membrane fabrication and performance. Accordingly, bridging the gap between performance and mechanistic insight offers a valuable framework for development of GO membrane design.

In this article, we provide a systematic investigation into the structure-property relationships of GO membranes fabricated from commercially sourced GO materials having distinct flake sizes. SFGO and LFGO coated polyethersulfone (PES) membranes were prepared using a vacuum filtration technique, their structure and morphologies characterised, and performance categorised according to a comprehensive experimental matrix. Cationic MB and anionic MO dyes were utilised to probe the nature of the GO membranes such that the role of charge and electrostatic interactions could be investigated. Furthermore, the potential application of the coated membrane systems to desalination was explored through testing of salt solutions comprising sodium chloride (NaCl), sodium sulphate (Na_2SO_4), magnesium sulphate ($MgSO_4$) and ammonium heptamolybdate ($(NH_4)_6Mo_7O_{24}$). Finally, selective dye-salt separation was investigated through filtration studies involving Na_2SO_4 and $MgSO_4$ dissolved in MB dispersions. Collectively, these experiments provide key insight into the governing flake-size dependent structure-property relationships in fabricated GO membrane systems and demonstrate the effectiveness these systems may have in treating multicomponent wastewater systems.

2. Experimental

2.1. Materials

Two graphene oxide samples were obtained from different commercial suppliers as 1.0 wt% dispersions in water. The GOs were extensively characterised, as detailed in our previous publication [45], revealing them to have significantly different median flake sizes (9.0 and 13.6 μm, as measured by laser diffraction techniques), for relatively similar surface chemistries. Hence, we termed these materials *smaller flake graphene oxide* (SFGO) and *larger flake graphene oxide* (LFGO). Aqueous anionic Methyl Orange (MO) at a supplied solution concentration of 0.10 wt%, and cationic Methylene Blue (MB) at 0.50 wt% dyes, and sodium sulphate ($Na_2SO_4 \bullet 10H_2O$), magnesium sulphate ($MgSO_4 \bullet 7H_2O$), sodium chloride (NaCl) and ammonium heptamolybdate ($(NH_4)_6Mo_7O_{24} \bullet 4H_2O$) salts were obtained from Merck (Germany). Additionally, 0.20 μm pore size, 47 mm diameter (effective membrane area 17.4 cm^2) polyethersulfone (PES) substrates were obtained from Sterlitech (USA). All chemical reagents and solvents were used without further purification or modification.

2.2. Preparation of GO/PES membranes via vacuum filtration

GO-coated PES membranes were prepared under identical experimental conditions *via* vacuum filtration techniques for both smaller flake (SFGO/PES) and larger flake (LFGO/PES) materials, labelled respectively throughout. The membrane fabrication process followed four sequential steps: *i.* GO dispersion dilution, *ii.* PES substrate preparation, *iii.* Vacuum filtration of GO onto the PES substrate and *iv.* ambient overnight drying of the GO-coated membrane. First, the GO dispersions were diluted in distilled water to a concentration range of 0.01 mg/mL and 0.10 mg/mL and sonicated in an ultrasonic bath at a nominal frequency of 35 kHz and bath power 100 W for 10 min to ensure a homogeneous dispersion. Second, a clean, dry PES membrane was carefully rinsed in distilled water, mounted on top of a vacuum filtration flask (Sartorius, Germany). Third, 7.6 mL of diluted GO dispersion was transferred by pipette onto the surface of the PES substrate. The flask was connected to a vacuum pump, which was switched on, resulting in deposition of GO onto the membrane surface, with the water passing into the vacuum flask. Finally, the coated, wet membrane was carefully removed using tweezers and dried at room temperature overnight in a covered petri dish.

Water uptake capacity of the uncoated PES and GO-coated membranes was investigated by immersing the membranes in 150 mL distilled water at room temperature and humidity for 24 h. The dry-state mass of the membranes was measured prior to immersion in distilled

water and water uptake percentage, $W(\%)$, was calculated by the relative difference in dry state mass (w_{Dry}) and hydrated state mass ($w_{Hydrated}$) of the membranes, according to Eq. 1 [46]:

$$W(\%) = \left(\left(w_{Hydrated} - w_{Dry}\right)/w_{Dry}\right)*100\% \quad (1)$$

2.3. Characterisation of GO/PES membranes

Fourier Transform Infrared (FTIR) analysis of dry membranes was performed using a Perkin Elmer (USA) spectrophotometer. Samples were mounted onto the attenuated total reflectance (ATR) crystal and the IR beam source directed at the sample. Spectra were recorded in transmission mode, in wavenumber interval 4000–400 cm^{-1}, with 32 scans at resolution 4 cm^{-1}. The background was corrected for analysis in air.

Thermogravimetric analysis (TGA) was performed using a simultaneous thermal analyser (Netzsch STA 449, Germany). Initial 47 mm diameter membrane samples were cut using a scalpel into round sections having mass 10 mg recorded using a 5 decimal place balance. TGA thermograms were recorded by heating the 10 mg samples from 30 °C–900 °C in a ceramic heating crucible with a ramp rate of 10 °C/min. Nitrogen was used as the purge gas, at a rate of 50 mL/min.

X-ray diffraction (XRD) analysis of the GO-coated membranes was performed using a Malvern Empyrean (UK) diffractometer with a CuK_α X-ray beam source ($\lambda = 0.154$ nm, beam power 30 keV, 10 mA). Analysis was conducted in the angular scan range $5° < 2\Theta° < 40°$, with step size 0.02°/min. Initial 47 mm membranes were cut using a scalpel into round shapes of 20 mm diameter and mounted onto a copper sample holder. The total scan time for each sample was 30 min. For all membranes, the positioning of peaks was converted to interlayer (d) spacing using the Bragg Eq. [47].

Water contact angle measurements were made using a tensiometer (Kruss Optronic GmbH, Germany). Static drop measurements were made at room temperature and humidity by dropping distilled water using a syringe onto each substrate to achieve consistently small droplets of approximate volume 2 μL. The droplets were imaged using a digital camera, and images were processed using OneAttension (USA) software. Contact angle calculations were made on the images by selecting the Young-Laplace option for drop shaping. Three measurements of water contact angle were made per substrate.

Cross sectional and morphological imaging of membrane samples was achieved using a Focused Ion Beam – Scanning Electron Microscope (FEI Helios G4 CX DualBeam, USA), equipped with a Ga^+ ion and electron beam. Samples were prepared for milling by sputter coating the surface with Pt^{2+} ions to protect the sample from burning. Following coating, the sample was secured on a silicon wafer using conductive carbon tape and transferred into a sample chamber evacuated to 10^{-9} bar for analysis. The ion beam, with power setting 30 kV, 20 nA, was directed vertically at the sample surface and steered to mill a trench in the sample of width 150 × 100 μm. Cross-sectional images were recorded by directing the 30 kV, 10 nA electron beam at the trench at angle 52° relative to the ion beam. Images were processed using *Auto Slice and View* software (Thermo Fischer, UK). GO coating layer thicknesses were estimated using an in-built tool in the software. Where possible, multiple measurements of thickness were made for each image.

2.4. Dead-end filtration testing of GO/PES membranes

The performance of the commercial GO-coated PES membranes were assessed for the removal of contaminants from water by filtration.

Here, *Rejection* in membrane science defines the percentage quantity of contaminant that the membrane can remove from the feed stream, relative to the initial amount. Thus, percentage rejection ($R\%$) may be calculated according to Eq. 2 [48]:

$$R\% = \left(1 - \left(C_p/C_f\right)\right)\cdot 100\% \quad (2)$$

where C_f and C_p (both mg/L) are the contaminant concentrations of the feed and permeate streams, respectively. Practically, UV absorbance and conductivity readings of the feed and permeate streams were used directly to calculate $R\%$, based on the assumption of a linear relationship between concentrations and UV absorbance of dyes, and between concentrations and conductivity of salts over the ranges utilised in this study.

Also, *Permeate flux* relates to the mass transfer of species (including water and unremoved contaminant) through the membrane. *Permeate flux* (J) ($L{\cdot}m^{-2}{\cdot}h^{-1}$) is defined by Eq. 3 [49]:

$$J = V_p/(A{\cdot}t) \quad (3)$$

where area A is the membrane cross-sectional area (m^2), V_p is permeate volume (L) and t is time (h).

Permeability (P) ($L{\cdot}m^{-2}{\cdot}h^{-1}{\cdot}bar^{-1}$) is equal to permeate flux scaled by operating pressure (*i.e.,* $P = J/p$, where p is operating pressure (bar)) [50]. In practice, all samples were measured by mass (g) which was directly converted into volume (mL), based on the assumption that the density of all dyes and salts solutions were 1 g/mL, across the range used in this study.

Dead-end filtration experiments were performed using a Sterlitech HP4750 (USA) filtration cell. Experiments were carried out by carefully transferring a membrane sample onto a wetted support disk, such that the entirety of the membrane covered the disk. The membrane was then placed in the base of the cell reservoir and tightly sealed by screwing inside the cell bottom using a 3-in. lower reservoir clamp. Contaminant solution was poured inside the cell chamber in direct contact with the membrane surface. The cell was positioned on a magnetic stirrer which was used to agitate the solution at constant speed (setting 5 on the instrument). A 2-in. reservoir clamp was used to close the top of the cell, which was then connected to a nitrogen gas cylinder (BOC 9.8 m^3, 230 bar, UK) for pressurisation. Inter-cell pressure was controlled *via* an external regulator by setting a constant desired pressure throughout the experiment. A 3 decimal places mass balance was positioned adjacent to the cell, with a collecting beaker such that permeating liquid could be collected and weighed. The time taken to collect certain masses of permeate was manually recorded using a stopwatch.

2.4.1. Dye filtration

MB and MO dyes were prepared at concentrations 5 or 10 mg/L by diluting in distilled water. These concentrations were selected so as to minimise aggregation effects and ensure linear UV–Visible detection by the spectrophotometer; they are typical of those found in GO dye rejection studies [48,51]. Following dilution, the dye solutions were magnetically stirred (stirring speed 3) at room temperature for a period of ten minutes. Initial measurements of UV absorbance were recorded using a UV–visible spectrophotometer (ThermoFisher Scientific Biomate 3, USA) operating for MB at 664 nm and for MO at 464 nm.

Filtration tests were carried out with an initial volume of 50 mL aqueous dye loaded into the cell. Following pressurisation, the mass output of permeate was manually recorded as a function of time. It was observed by experiment that after the pressure was set there was an initialisation period in order for the permeate flux to reach steady state, with droplets amassing at regular intervals. The timer was started when the flux steadied, and the time taken for each gram (mL) of permeate was recorded. For every 4 g of permeate collected the UV absorbance was recorded. The procedure was iterated in this fashion until 20 mL had permeated through the cell.

The permeating volume at each mL was converted to P at each mL and the $R\%$ calculated at each 4 mL according to Eq. 1 with the value of C_f taken as the initial reading of UV absorbance of the prepared dye solution.

2.4.2. Desalination using GO/PES membranes

Aqueous salt solutions of sodium chloride, sodium sulphate,

magnesium sulphate and ammonium heptamolybdate were prepared at initial concentrations of 0.50 g/L. The electrical conductivity of the prepared salt solution was measured using a portable conductivity meter (Hach HQ1130, UK), providing a reading for C_f. The salt concentrations employed in this study were selected to facilitate mechanistic comparison and understanding of ionic transport behaviour in GO membranes, rather than to replicate the salinity of seawater or industrial brines, which may typically be much higher.

The procedure was analogous to that of the dye filtration experiments (above), in which 20 mL was permeated through the membrane, with permeability calculated every mL and conductivity measurements recorded every 4 g.

2.4.3. Fractionation of dye-salt mixtures using GO/PES membranes

Experiments regarding the fractionation of dye-salt mixtures were performed using MB/sodium sulphate and MB/magnesium sulphate mixtures. Dye-salt solutions were prepared by taking a 5 mg/L MB solution in distilled water (procedure discussed in Section 2.4.1), and dissolving the salt using the same mixing procedure to obtain a salt concentration in MB of 0.50 g/L.

Initial measurements of UV absorbance at 664 nm and electrical conductivity were recorded. An analogous procedure to the dye filtration and desalination experiments (above), with an initial feed volume of 50 mL was undertaken. Fractionation experiments were conducted at 2 bar. For every 4 mL permeated, measurements of UV absorbance and conductivity of the permeate were recorded, thus enabling separate calculations of dye and salt rejections at each stage. It was assumed that the conductivity of dyes and UV absorbance of salts are negligible for the concentrations range used in this study. Measurements of permeated volume were also made in 1 mL increments.

3. Results and discussion

3.1. Characterisation of GO/PES membranes

Characterisation of SFGO and LFGO produced GO/PES membranes at two different mass loadings (0.01 and 0.1 mg/mL) are presented in Fig. 1, showing (a) Fourier Transform Infrared (FTIR) spectroscopy, (b) Thermogravimetric Analysis (TGA), (c) X-ray Diffraction (XRD), and measurement of (d) Water Contact Angle and Water Uptake percentage (*W(%)*).

FTIR analysis (Fig. 1a) of the pure membrane showed the presence of characteristic PES peaks located at 1578 cm^{-1}, 1484 cm^{-1}, 1240 cm^{-1} and 1152 cm^{-1}, which were assigned as C═C, C—H, C—O and S═O functional groups, respectively [52]. Traces of GO-coated substrates were identical to that of pure PES. Recorded wavenumber positions for any peaks identified for PES were not shifted in position by application of the GO coating, and the magnitude of peak intensities were neither diminished nor enhanced. Due to the low concentration of GO used, corresponding signals were found to be very weak in comparison to those of PES, confirming that GO was acting as a filler material and was not interacting chemically with the substrate. Similar observations were made by Ali et al. [53], in which GO was deemed to act as a filler material in the GO-PES membrane, exhibiting no chemical interaction with the membrane.

The thermal response of all materials was investigated by TGA (Fig. 1b), which revealed similar thermal profiles for both the pristine substrate and the GO composite membranes. TGA profiles revealed that membrane degradation occurred in a single loss-of-mass stage, ultimately leading to sample degradation. Insignificant losses (<10%) were observed for all membranes up to approximately 520 °C; these may be attributed to residual solvent evaporation from the sample [54].

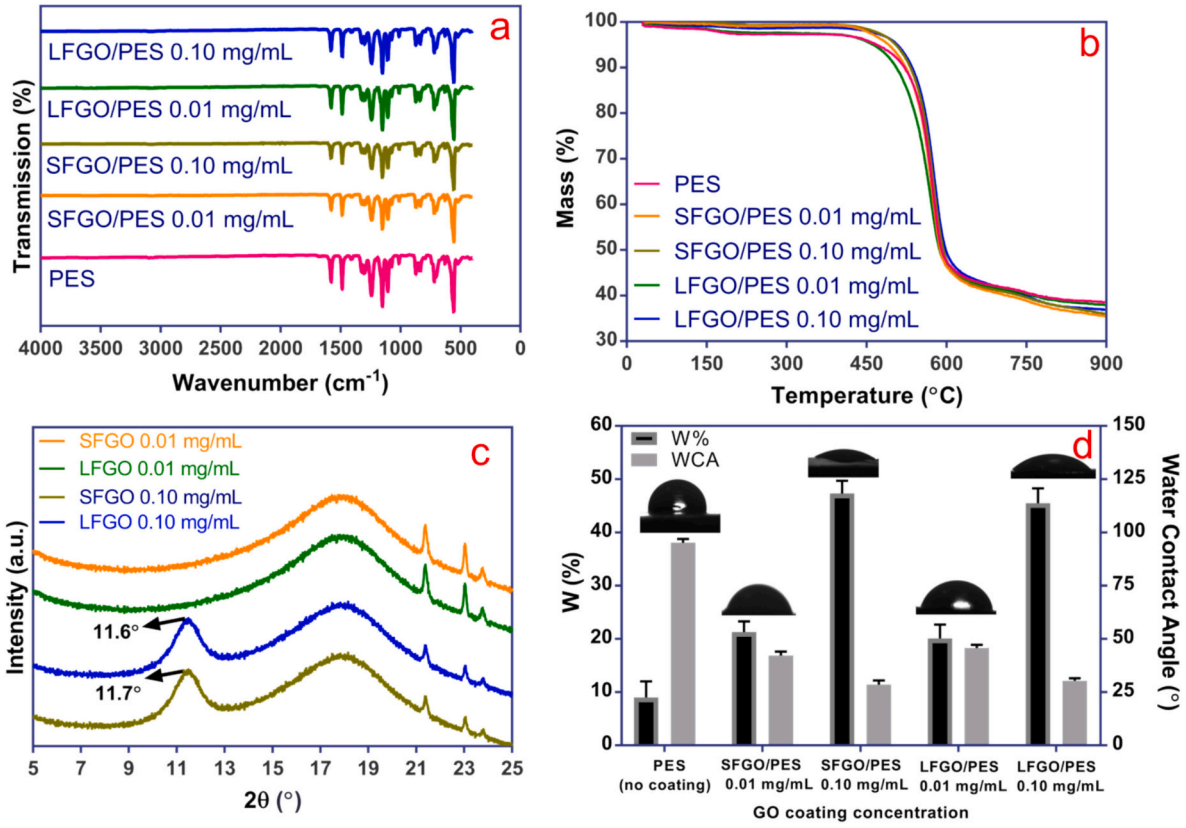

Fig. 1. Characterisation of SFGO/PES and LFGO/PES membranes at two different mass loadings of GO (0.01 and 0.10 mg/mL) by (a) Fourier Transform Infrared (FTIR) spectroscopy, (b) Thermogravimetric Analysis (TGA), (c) X-ray Diffraction (XRD), and (d) Measurement of Water Contact angle and Water Uptake percentage (W(%)).

Significant depletion of mass, however, occurred in the temperature range 520–600 °C due to thermal degradation of the polymer chains resulting in expulsion of gases, likely including oxides of carbon [55]. Temperature elevation above 600 °C resulted in flattening of the degradation profiles and, as the temperature reached the upper experimental limit of 900 °C, a stable carbonaceous ashen material remained [56]. The temperature at which mass loss from a sample is 3% ($Td_{3\%}$) is typically used for defining the thermal stability of a material [57]. For each membrane, the $Td_{3\%}$ value was estimated: PES (414.6 °C), SFGO/PES 0.01 mg/mL (466.2 °C), SFGO/PES 0.10 mg/mL (483.3 °C), LFGO/PES 0.01 mg/mL (416.1 °C) and LFGO/PES 0.10 mg/mL (482.5 °C). Although the overall thermal profile was dominated by PES, increasing the GO loading resulted in an increase in $Td_{3\%}$, thus indicating that GO deposition improved the thermal stability of the composite membrane. This improvement is thought to be as a result of the strong adhesive forces at the interface between the PES membrane and coating GO layer, which enhanced the ability to remain intact when subjected to elevated temperatures [58].

XRD analysis (Fig. 1c) was utilised to calculate the interlayer spacing of the dry-state GO-coated membranes. The patterns of all four samples revealed a very broad, hump-like peak centred on $2\Theta = 18°$ attributed to the underlying PES substrate [59]. Two very low intensity peaks were observed at $2\Theta = 21.4°$ and 23.0°, which were attributed to the copper sample holder. The two lower concentration GO membranes did not appear to show distinguishable XRD intensities in the typical GO region ($2\Theta \approx 11°$). The two 0.10 mg/mL GO samples displayed broad peaks around 11°, as indicated on the separate diffraction patterns, and these may be ascribed to the presence of the GO coating. For the LFGO membrane the peak was positioned at $2\Theta = 11.7°$, corresponding to an interlayer d-spacing of 0.76 nm as determined using the Bragg Equation (Section 2.3). Analogously, for SFGO, the peak was positioned at $2\Theta = 11.6°$ (interlayer spacing 0.76 nm). It was considered that the lower loading of GO (0.01 mg/mL) resulted in a membrane structure possessing overall lower levels of disorder, therefore having a diminished impact upon XRD scattering and resulting in a diffraction peak of negligible intensity [60]. The peak positions and associated d-spacing values for the GO/PES membranes were consistent with other studies involving GO membranes prepared by vacuum filtration methods, in which interlayer spacings of 0.80 ± 0.10 nm are typical [61,62].

As discussed, GO has hydrophilic functionality which is a feature credited to its decoration with hydrophilic groups including epoxy, carbonyl and carboxylic groups [14,63]. Measurement of the water contact angle was used to assess surface hydrophilicity, where values >90° indicate hydrophobicity and < 90° hydrophilicity [64]. In Fig. 1d, the water contact angle and uptake percentage (*W(%)*) is shown for each of the GO-coated membranes and for PES. Representative images of water droplets on the GO surface captured during measurements are also shown. In bulk form, PES is weakly hydrophilic, however, the measured water contact angle of the membrane exceeded 90°, a feature arising from its porous and rough surface morphology. Owing to this surface roughness, air can become entrapped beneath the water droplet, leading to an artificial increase in the measured water contact angle. The low *W(%)* demonstrated limited capacity to absorb water. Application of a GO coating onto the polymer had the effect of significantly increasing hydrophilicity and reducing the water contact angle of the membrane. A higher concentration of GO resulted in greater reduction (and so greater hydrophilicity) due to the greater presence of hydrophilic groups which lower interfacial tension [65]. Meanwhile, it was observed that increasing GO concentration from zero (pristine PES) to 0.10 mg/mL had the effect of increasing *W(%)* as the membrane had greater functional group capacity for water absorption. As such, there was an inverse relationship between water contact angle and *W(%),* a feature previously observed in the literature [66]. In our previous work [45], XPS revealed LFGO contained a higher oxygen content than SFGO. Interestingly, in this study, SFGO membranes at both concentrations were shown to have lower contact angles than their LFGO counterparts, therefore implying SFGO membranes were more hydrophilic. It is suggested that overall oxygen content may have poor correlation with hydrophilicity, as in these cases, the slightly higher content in LFGO did not result in greater hydrophilicity. This change in effect may be because different hydrophilic groups (*e.g.* epoxy, carbonyl and carboxylic groups) contribute differently to the hydrophilicity of the GO membranes.

When GO materials are contacted with water the interactions between the hydrophilic GO groups and water leads to intercalation within the GO structure [33,63]. In the case of the above, this effect was found to result in an increase in *W(%)*. When coated membranes are prepared using an uncontrolled layer stacking technique such as vacuum filtration, the stacked GO sheets are held together by weak Van der Waals' forces and, due to uptake of water, these layers may experience a swelling effect [34,67]. Such physical changes are a significant hindrance in the utility of GO materials to desalination, in which the ionic species are of sub-nanometric size and may thus be small enough to permeate the swollen nanochannels [36,38,68]. Thus, XRD analysis was utilised to investigate the phenomenon of GO layer swelling by determining changes in interlayer spacing when the membranes were in a hydrated state. The diffraction patterns are shown in Fig. S1 of the Electronic Supplementary Materials (ESM). Again, no GO peak was observed on the 0.01 mg/mL samples, but the 0.10 mg/mL GO samples showed a shift in peak position: for SFGO to 11.1° and for LFGO to 10.8°, translating to interlayer spacings of 0.80 and 0.82 nm, respectively. It may therefore be concluded that water uptake resulted in an expansion of the interlayer spacing, with the potential implications considered in Section 3.3.3.

Fig. 2 shows the morphology and cross section of GO-coated PES membranes, as imaged using Focussed Ion Beam Scanning Electron Microscopy (FIBSEM). A morphological image of the pristine PES membrane is shown for reference in Fig. S2. Pristine PES was revealed to be highly porous, with large open surface pores clearly evident.

The application of GO coatings to PES had a significant impact on the morphology of the substrate. SFGO/PES 0.01 mg/mL (Fig. 2a) appeared to offer near complete coverage, although a number of underlying pores remained visible. Morphologies of the 0.10 mg/mL SFGO (Fig. 2b) and 0.01 mg/mL LFGO (Fig. 2c) coatings revealed complete coverage, with no visible PES pores. These coatings appeared to be uniform and tightly packed across the surface of the membrane, albeit with striations in the GO coating effect. The 0.10 mg/mL LFGO coating (Fig. 2d) also appeared to offer complete coverage, however the coating did not appear uniform with large lateral distortions on surface regions clearly visible at the 1 μm scale. It is proposed these regions resulted from aggregated layers of GO [69].

Cross-sectional imaging of the coated membranes (Fig. 2a' – d') showed the deposition of GO onto PES. Cursory inspection of the images revealed the GO to be layered on top of the underlying PES substrate. The introduction of porous features into the polymeric film is a feature of the membrane manufacturing process of phase inversion and, as such, the pores were laterally observable in cross-sectional analysis. Due to the blockading effects of the GO coating there appeared to be no uniform pathway through which contaminant species or water may permeate. The somewhat randomly packed nature of polymeric membranes has been observed in the literature using SEM analysis [70,71]. The GO coatings themselves appeared ordered and compacted, spread across the PES surface. The coating layer dipped randomly along the path, suggesting that the layer had encountered a PES pore. It is, however, not evident from the images that GO was penetrating the substrate pores since below the coating layer only the PES lamellae were visible. This is consistent with expectation, given the relatively large size of the GO flakes in relation to the 0.20 μm pores on the PES substrate (noting previous SFGO and LFGO size estimates [45]).

Estimates of GO layer thickness were made in accordance with the thicknesses observed in cross-sectional imaging and, perhaps unsurprisingly, were shown to be positively related to GO concentration. The

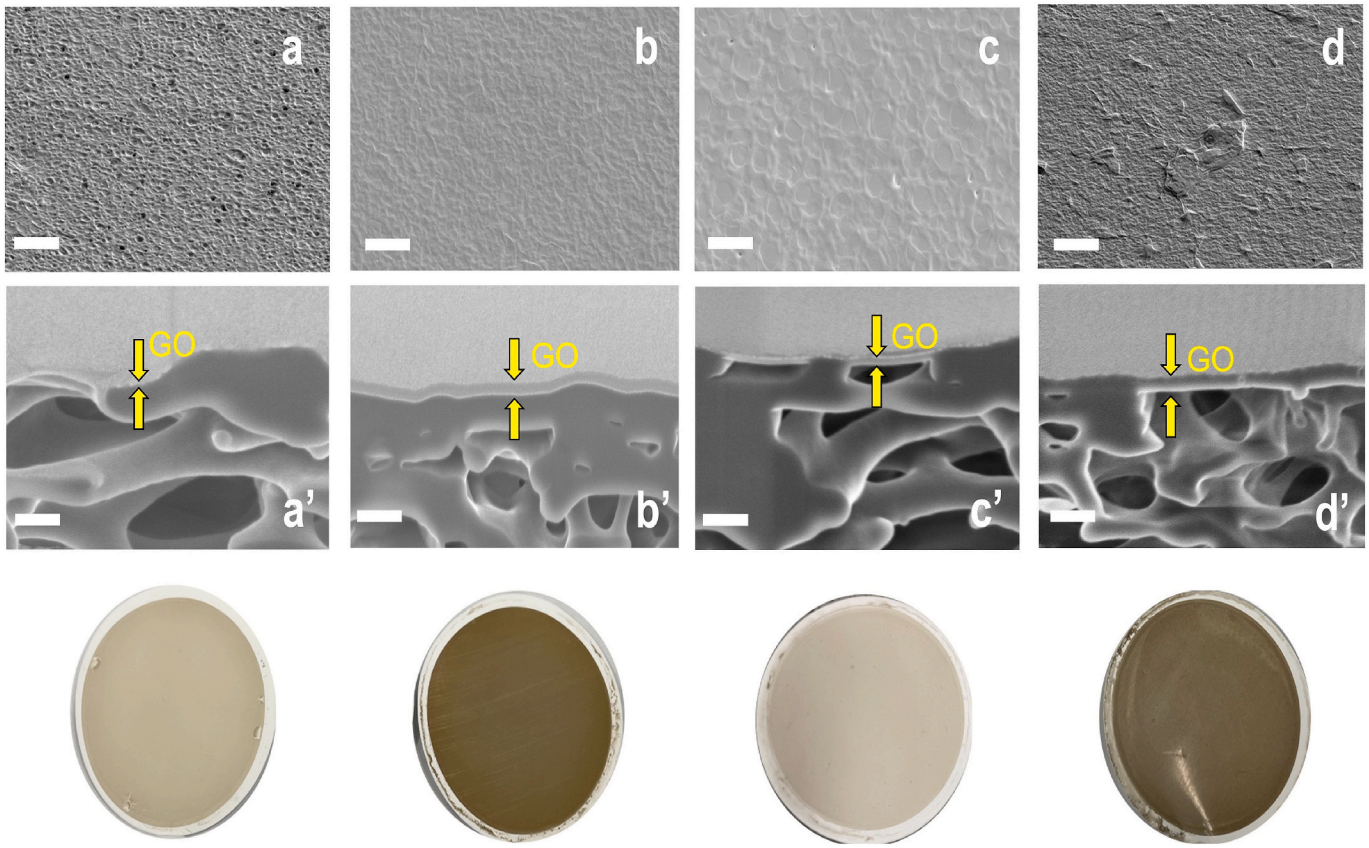

Fig. 2. FIBSEM images of GO-coated membranes: (a) SFGO/PES 0.01 mg/mL, (b) SFGO/PES 0.10 mg/mL, (c) LFGO/PES 0.01 mg/mL, and (d) LFGO/PES 0.10 mg/mL. The dashed counterparts show the corresponding cross-sectional images of the respective membranes. All scale bars represent 1 μm. Coated membrane samples are shown at the bottom and correspond to membranes a – d, respectively.

mean layer thicknesses, including standard deviation error, were: SFGO/PES (0.01 mg/mL) 26.0 nm, SFGO/PES (0.10 mg/mL) 72.0 ± 6.8 nm, LFGO/PES (0.01 mg/mL) 25.7 ± 3.7 nm and LFGO/PES (0.10 mg/mL) 167.8 ± 5.6 nm (Note that the mean GO layer thicknesses were calculated from the obtained images. For clarity, the measured thicknesses for each image are included in Table S1 of the ESM). It was noteworthy that increasing the GO concentration by factor of ten (*i.e.*, from 0.01 to 0.10 mg/mL dispersion) for SFGO and LFGO did not result in a tenfold increase in layer thickness; for SFGO the factor of increase was 2.67, and for LFGO it was 6.53. It has been suggested that higher GO concentrations result in coatings with greater microstructural density than lower concentration coatings [59,72]. An interesting question remains as to why the LFGO membrane at higher concentration was significantly thicker than its SFGO counterpart, especially given the interlayer spacing revealed by XRD analysis was almost identical for both membranes (Fig. 1c). It is hypothesised that the smaller SFGO flakes were able to stack with increased density on the substrate resulting in a thinner, more compacted coating layer. Conversely, thickness data suggested the LFGO had a greater resistance to compaction, which is potentially advantageous since it indicated the structure was better maintained with higher loadings.

3.2. Removal of dyes using GO/PES membranes

3.2.1. Impact of initial dye concentration

The impact of initial dye concentration upon filtration performance was evaluated by preparation of 5 and 10 mg/L Methylene Blue (MB) and Methyl Orange (MO) dyes and performing filtration tests using PES and GO-coated PES membranes.

Mean permeability and dye rejection (%) for PES are summarised in Table S2 in the ESM; standard deviation error in permeability and rejection across three experimental runs is also provided in the table. The uncoated PES membrane was shown to exhibit negligible rejection of either dye, with mean rejections in all cases <2%. Permeabilities were also very high, further indicating that the uncoated membrane offered practically no resistance to the permeation of dye molecules. Given the size disparity between dye molecules having lateral dimensions <10 nm and the 0.20 μm PES membrane pores, it was considered physical size sieving was unlikely to be an effective mechanism of separation. This was consistent with other dye rejection studies using polymeric filters [73].

Results achieved in 5 and 10 mg/L MB and MO removal experiments using the 0.01 mg/mL SFGO/PES and LFGO/PES systems is shown in Fig. 3. The effect of application of the GO coating was apparent as permeabilities (flux per unit pressure) were reduced by an order of magnitude relative to the results for uncoated PES (see comparison with Table S2). Meanwhile, all systems exhibited step increases in dye removal. The analogous results for the 0.10 mg/mL GO coating systems experiments are presented in Fig. S3 of the ESM. As discussed earlier, localised variations in GO stack thickness are an inherent feature of vacuum filtration coating techniques. The reproducible performance trends observed suggest, however, that such variations did not obscure the influence of GO flake size on membrane behaviour thus indicating good consistency in membrane fabrication.

For all systems, increasing initial cationic MB concentration in the feed from 5 to 10 mg/L resulted in a decrease in both overall mean permeability and MB rejection. The presence of a higher initial dye concentration in the feed gave rise to a more substantial concentration gradient, as the concentration of solute (dye) is initially higher, resulting in greater osmotic pressure [74]. This gradient gives rise to an effect

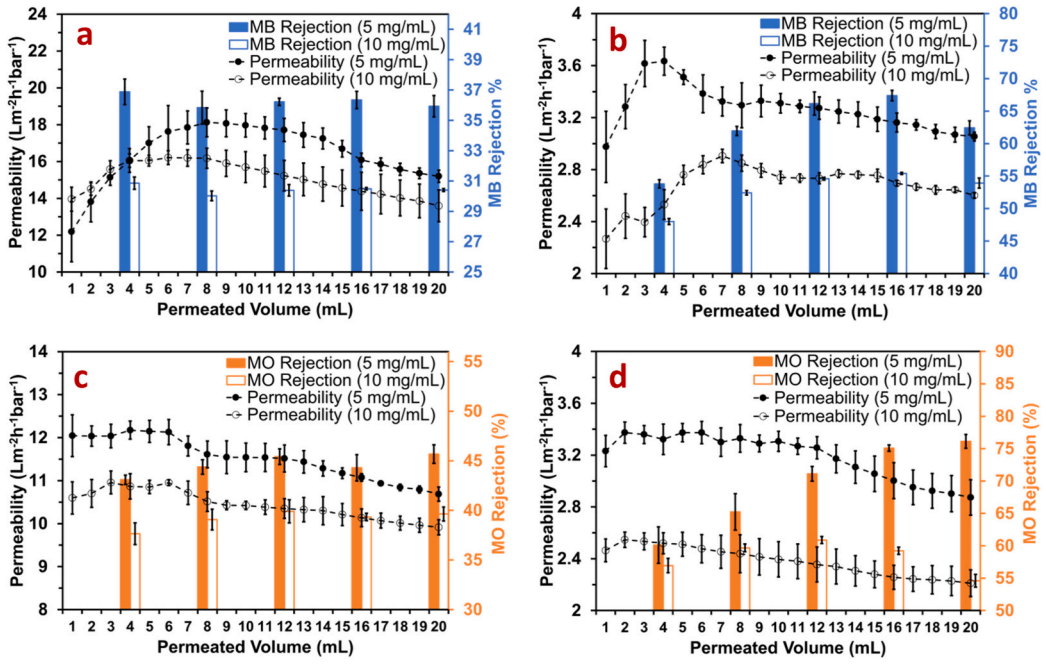

Fig. 3. Permeability and dye rejection of 5 and 10 mg/L MB solutions using (a) 0.01 mg/mL SFGO/PES, and (b) 0.01 mg/mL LFGO/PES membranes as a function of permeated volume. Similarly, permeability and dye rejection of 5 and 10 mg/L MO solutions using (c) 0.01 mg/mL SFGO/PES, and (d) 0.01 mg/mL LFGO/PES membranes under identical pressures and dye concentrations. Vertical error bars represent standard deviation over three separate runs.

known as concentration polarisation, in which solute concentration gradient was principally responsible for the decline in effective mass transport of solvent [75]. In prolonged periods of operation, the membrane showed greater tendency to become fouled by higher dye concentration, resulting in an overall decline in efficacy of performance [76].

Similarly, anionic MO mean permeabilities and mean levels of MO rejection were shown to follow a comparable trend compared with MB. It is proposed that this results from the higher initial dye concentration resulting in greater levels of concentration polarisation. Mean permeabilities were slightly lower in MO filtration, while relative rejections were slightly higher compared to the filtration of MB. This difference is considered to be a feature of the sensitivity of the GO coating in interaction with cationic/anionic dyes, although this phenomenon is discussed further in Section 3.2.5.

An interesting observed feature was that the SFGO systems offered significantly higher permeability when compared to the analogous LFGO systems. Typically, the permeability of the SFGO systems was a factor of four greater for both dyes compared to LFGO. This property was particularly noteworthy given that the GO coating thicknesses of these membranes was very close, as measured using FIBSEM (Fig. 2). This behaviour is consistent with other studies which investigated the impact of flake size on solvent permeation rates [41,77,78]. The smaller flake sizes enabled the creation of shorter transport pathways during preparation by vacuum filtration, facilitating the channelling of solvent through nanochannels, thus resulting in higher permeabilities of the SFGO systems [79]. Although the dye concentrations selected for these studies were 5 and 10 mg/L, the observed trends in permeability and rejection are consistent with similar GO membrane studies using higher initial dye concentrations [80,81].

3.2.2. *Impact of GO coating concentration*

The impact of GO dispersion concentration in coating was evaluated by considering the removal of 5 mg/L MB and MO solutions with GO loading concentrations of 0.01 mg/mL and 0.10 mg/mL. The mean permeabilities are shown in Fig. 4a, and the mean dye rejections in Fig. 4b. These results were obtained in correspondence with Fig. 3 (and Fig. S3) by extracting the 5 mg/L results. The vertical error bars show

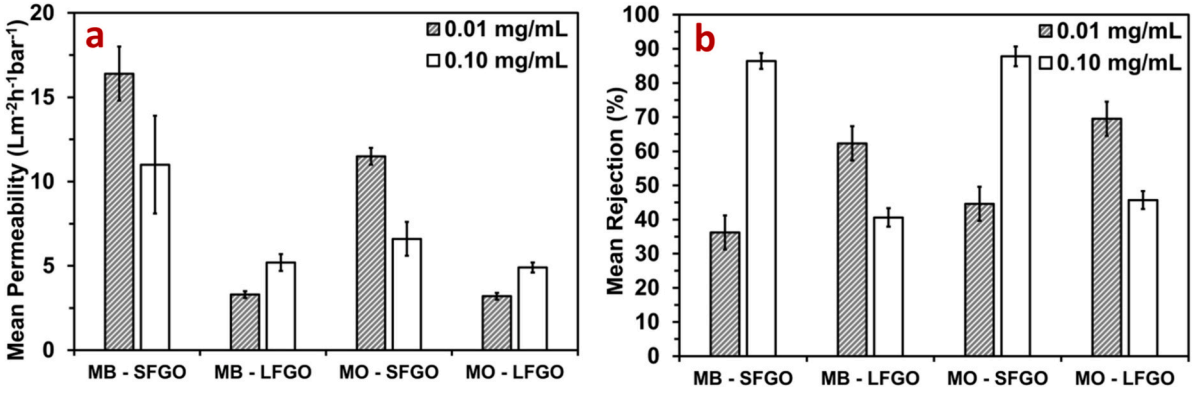

Fig. 4. (a) Mean Permeability, and (b) Mean dye rejection achieved in filtration of 5 mg/L MB and MO dyes using 0.01 mg/mL and 0.10 mg/mL dispersion concentrations of commercial GOs in preparation of coating. Vertical error bars represent standard deviational error across three separate runs.

the standard deviation error across three separate experimental runs.

For the SFGO/PES coatings, it was determined that an increase in GO concentration resulted in a reduction in overall permeability, accompanied by a significant increase in rejection performance. The transport of permeant in polymeric membrane systems is inversely related to membrane thickness [82] and, as such, increasing the GO concentration resulted in thicker coatings, decreased permeability and increased rejection [83]. This was principally due to the overall increase in mass transfer resistance induced by the thicker GO layer [84]. However, with reference to Fig. 2, it was known that the thicker layer was substantially more dense and potentially less porous. In addition, it is possible that the greater quantity of GO in the coating was leading to flake aggregation such that nanoporous features of the coating were narrowed by the aggregates, which in turn may have reduced permeability [85].

Interestingly, for the LFGO/PES coatings, the relationship between the GO concentration, permeability and dye rejection was in contrast to that of the SFGO/PES membranes. It was found that increasing the LFGO concentration led to greater permeability and poorer rejection of both dyes. This behaviour does, however, show consistency with other studies [86,87], in which improvements in hydrophilicity were considered responsible for an increase in solvent permeability subject to decreasing water contact angle. Nonetheless, it was interesting that the LFGO/PES system should demonstrate such a trend, as it was determined that the layer thickness of the LFGO/PES systems increased very significantly when coating concentration was increased. As demonstrated by the FIBSEM analysis of the membrane cross sections, the thicknesses were typically more than a factor of two greater for the 0.10 mg/mL LFGO loadings *versus* the SFGO (Fig. 2).

In order to investigate the solvent stability of all membranes, and to gain further insight into the somewhat surprising behaviour of the LFGO/PES system, dried samples of the GO-coated membranes were subjected to a 24-h immersion period in distilled water. Images of the dry and hydrated state membranes are shown in Fig. S4 in the ESM. This investigation showed the LFGO/PES 0.10 mg/mL sample was unable to remain intact, as regions of the coating peeled off following immersion exposing the underlying PES substrate. These regions are expected to permit enhanced dye and solvent permeation as the PES membrane offered very limited rejection of dyes. As such, poor solvent stability of the 0.10 mg/mL LFGO coating would be a major contributing factor accounting for the observed high permeability and low rejection. An interesting extension of the study would be to trial different polymeric substrates including, for example, polyamide, polyether ketone or polyvinylidene fluoride. These alternatives could eliminate possible side reactions of GO with the polymeric membrane which may be occurring in the case of LFGO with PES, and would also provide further exploration of the role of the underlying polymer within coated systems. Furthermore, while the immersion stability test provided key insight into the overall robustness and durability of the GO coating under hydrated conditions, quantitative mechanical testing and long-term performance testing were not undertaken as part of this study.

3.2.3. *Impact of filtration pressure*

The impact of filtration pressure upon removal performance was investigated using 5 mg/L MB and MO at maintained pressures of 2 and 4 bar, as presented in Fig. 5. The results of the 2-bar filtration experiments corresponded to those in Section 3.2.1. Filtration results are presented for MB using (a) 0.01 mg/mL SFGO/PES and (b) 0.01 mg/mL LFGO/PES systems, and for MO removal in the (c) 0.01 mg/mL SFGO/PES and (d) 0.01 mg/mL LFGO/PES systems. The analogous results for 0.10 mg/mL GO coating systems are presented in Fig. S5 of the ESM.

For both dyes it was seen that increasing pressure from 2 to 4 bar resulted in an overall increase in permeability and corresponding steep decrease in rejection capabilities for both the SFGO/PES and LFGO/PES systems. The permeability for the SFGO/PES systems was still significantly higher compared to their LFGO/PES counterparts at both pressures.

In coated membrane fabrication techniques such as vacuum filtration, the GO flakes may not stack in an ordered fashion due to vacuum

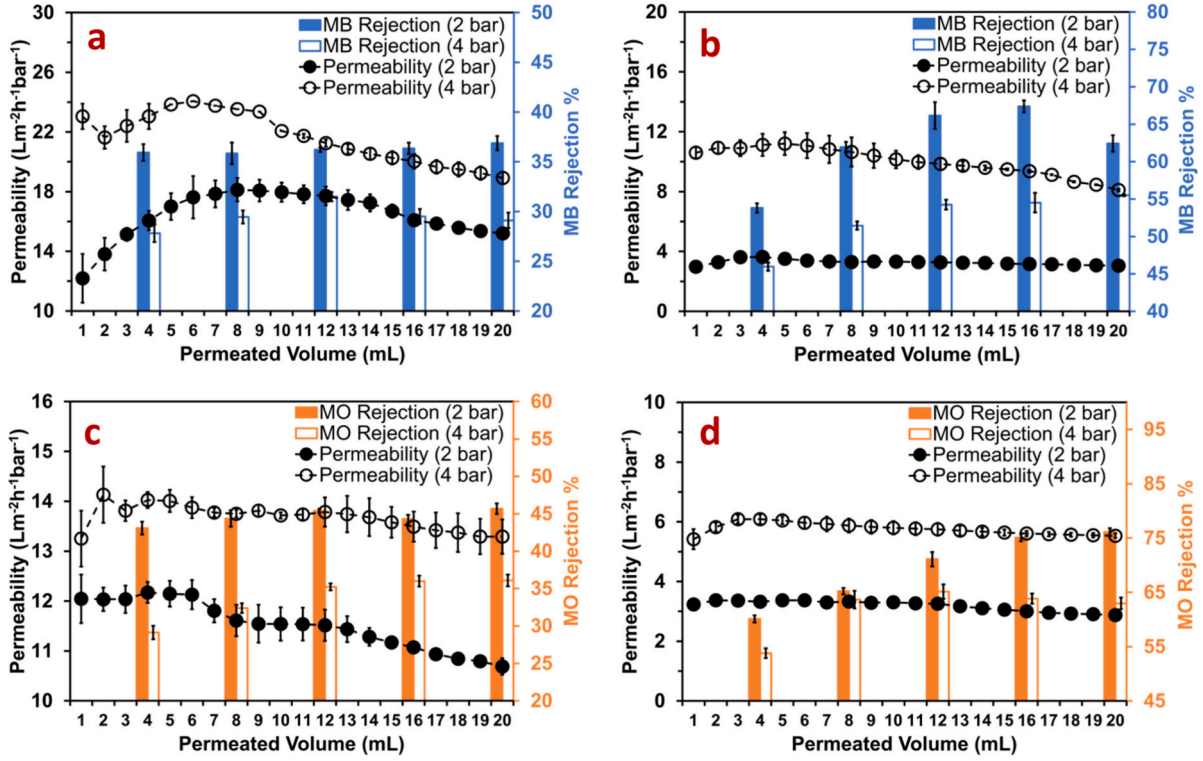

Fig. 5. Permeability and dye rejection of MB using (a) 0.01 mg/mL SFGO/PES, and (b) 0.01 mg/mL LFGO/PES membranes as a function of permeated volume with initial dye concentration of 5 mg/L at respective pressures 2 and 4 bar. Additionally, permeability and dye rejection of MO using (c) 0.01 mg/mL SFGO/PES and (d) 0.01 mg/mL LFGO/PES membranes under identical pressures and dye concentrations. Vertical error bars represent standard deviation over three separate runs.

effects [88]. In particular, the uppermost layers of the coating material may become loosely packed due to weakening of the vacuum suction forces with increasing distance from the substrate surface [89]. These microstructural defects, resulting from the somewhat random stacking of GO layers, are an inherent feature of such coatings [90]. The observed changes in permeability and dye rejection at higher operating pressures suggests that the microstructural defects may become more prominent under such conditions. While direct nanoscale characterisation of membranes under elevated pressure was not performed, this interpretation is consistent with the known response of GO membranes to operation under higher pressures [91]. A number of existing studies have, however, suggested that increasing filtration pressure resulted in the collapse of nanoporous morphological features, thereby closing channels and resulting in increased dye rejection and decreased permeability [92,93]. It appeared in the current GO/PES systems that the effects of the defects were, nonetheless, influential in defining behaviour at higher pressure. In particular, the increased pressure had a greater impact on the permeability of the LFGO/PES systems, which may suggest the defects were more emphatic as a consequence of the larger flake size.

3.2.4. Reusability of GO membranes

The issue of reusability of GO membranes is a highly salient topic attracting significant research interest [20,94,95]. As discussed above, the adsorption of dye molecules onto the surface may hinder membrane performance thus restricting operational longevity due to diminishing permeate flux; a phenomenon often referred to as fouling [96,97]. In the continuing development of GO membranes, the capability to withstand blinding due to dye molecules, and therefore enhance reusability for further filtration cycles is an important objective. Membrane regeneration for further use improves the environmental and economic prospects associated with life cycle [98]. Although reusability and cleaning strategies are critical for practical application of GO membranes, systematic evaluation of flux and rejection recovery following cleaning processes was beyond the scope of the present study. Several studies have, however, demonstrated effective regeneration of GO membranes through simple solvent washing protocols. Subrahmanya et al. [99] found that washing GO polymer membranes with ethanol was able to maintain MB rejection at over 99% after three cycles, but this dropped to 87% after the fifth run. This suggested that membrane performance was maintained at high levels despite persistent reuse. A further study, by Kandjou et al. [100], also utilised ethanol as a cleaning agent, reporting that flux declined very little from 1.8 $L{\cdot}m^{-2}{\cdot}h^{-1}$to 1.74 $L{\cdot}m^{-2}{\cdot}h^{-1}$ over six operational cycles.

Table S3 provides a literature summary of the performance of a number of polymeric membranes, including GO or GO-composite based systems, in addition to alternative polymer or modified substrates in dye removal [101–106]. Where possible, permeability achieved, dye rejection capability and operational conditions at which the study was performed have been included. Dye charge at neutral pH is also indicated in the table, where (+) and (−) represent cationic and anionic dyes, respectively. The results obtained for the top performing candidate in our study (SFGO at 0.10 mg/mL loading) are likewise provided in the table. In summary, it appears the results obtained in our study regarding the removal of MB and MO are consistent with examples of polymeric membrane fabrications from the literature, which is significant given the development of GO membranes. There does however appear to be significant disparity in performance between the different studies, which is undoubtedly related to the unpredictable nature of the material and experimental conditions. It is worth noting that some of the best performing composite membranes are significantly more complicated to produce, with greater barriers to industrial implementation, than the vacuum deposited GO-PES membranes in the present study.

3.2.5. Discussion: Mechanism of dye removal

In this section, we seek to establish an understanding of the filtration mechanism which governs the permeability and dye rejection performance of the membranes. This is essential for developing a complete framework for the behaviour of the system. In GO systems, the ionic charge of the dye is considered to have a significant interaction impact. The GO itself possesses negative charge characteristics owing to the numerous oxygenated functional groups, as previously discussed [12,107]. The zeta potential of the GOs used in these studies, at respective concentrations of 0.01 and 0.10 mg/mL in distilled water and neutral pH, are shown in Fig. S6 in the ESM. This confirms the electronegativity of the materials and of the membrane coatings. This is a highly important feature in the interaction of GO with cationic MB and anionic MO dyes. Both dyes are of similar molecular size and, as such, steric hindrance is considered similar.

The removal of cationic dyes such as MB by GO membranes has been proposed to take place in a two-stage mechanism [22]. The first stage consists of cationic dye surface adsorption, and the second stage involves interactions between dye and surface such that the dye molecules may remain bound to vacant sites, including through $\pi - \pi$ interactions. Accordingly, adsorption is an important feature in the removal of dyes, however the overall separation mechanism in GO membranes should be interpreted in the context of coupled transport phenomena rather than as an independent equilibrium process. The electronegativity of the GO surface is an important aspect for facilitating the adsorption of cationic dyes. This feature is particularly important given the low concentrations of dyes used in the feed solution (5 or 10 mg/L), where adsorption onto the surface can significantly enhance the observed dye removal. To highlight the extent of the adsorption stage during filtration of MB, a GO-coated membrane is shown in Fig. S7 within the ESM. The change in colour of the coating from brown to blue emphasises the significant quantity of MB that adsorbs onto the surface during filtration. As discussed in the previous section, this behaviour may adversely impact the longer-term operational efficacy of the membranes.

In our previous work [45] we performed studies of dye adsorption using aqueous dispersions of GO adsorbents with different flake size. By analogy to our studies here, MB and MO were selected as investigation dyes. It was determined that the overall quantity of dye adsorbed by the GO as a function of time (q_t) increased for both dyes throughout the duration of the experiments, and that the SFGO material was particularly effective in adsorption of MB due to its high zeta potential, small flake size and high surface area. It was therefore consistent that the 0.10 mg/mL SFGO coating was the most effective in removal of MB since it had the greatest surface area and pore volume availability to adsorb MB molecules, coupled with a high capacity for sorption. Another interesting feature was that dye rejection percentages were found to increase as a function of time, especially for membranes with higher GO loadings (Fig. 3, Fig. 5); this was in analogy to the aforementioned increase in q_t and suggests that the interaction of coating with MB was intrinsically related to adsorption capacity. During extended periods of operation dye molecules were continually adsorbed onto the membrane coating until the coating reached a state of maximal adsorption in which the electronegativity was eliminated [108]. It was postulated that beyond the state of adsorption maxima, the membranes rejection may begin to decline due to the effects of fouling [109] (although this was not observed over the timescales utilised in this series of experiments). Permeabilities of all membranes were found to be initially high, followed by a gradual reduction as more liquid volume permeates over time. Under the dead-end filtration configuration conditions employed in this study, permeability decline is likely driven by a combination of membrane fouling attributed to adsorption, concentration polarisation, and pressure-induced structural modifications within the GO coating layer. Individually, these contributions cannot be readily decoupled using the present experimental design, and no single dominant mechanism is therefore claimed. To more precisely elucidate the mechanism of permeability decline a different experimental framework would be required, for example comparative dead-end and cross-flow filtration, to evaluate the contribution of concentration polarisation and fouling,

together with microstructural characterisation before and after filtration to probe potential structural changes. Performance recovery following membrane cleaning was not assessed in this study. Such investigations would provide a more definitive mechanistic understanding and are identified as important directions for future work.

In filtration studies involving anionic MO, electrostatic repulsion between negative charges has been considered a principal feature in the rejection mechanism [13,110]. Dye adsorption studies in our previous work showed both SFGO and LFGO to be significantly poorer adsorbents of MO in comparison to MB (the more electronegative SFGO/PES system was also poorer than LFGO/PES in adsorption of MO). It was thus considered that the adsorption phase of rejection, as discussed above, was comparatively minimal compared to the filtration of cationic MB. Nevertheless, adsorption interactions between GO and MO are possible due to $\pi - \pi$ interactions [111], although this feature was considered weaker than the strong electrostatic attraction between GO and cationic MB. The GO membranes did, however, appear by inspection to adsorb MO molecules as indicated by the orange colouration to the post-filtration GO surface (Fig. S7 in the ESM).

Interestingly, comparison of filtration results between MB and MO indicated a gross overall similarity in which permeability tended to reduce as a function of permeated volume, whereas rejection increased. It is therefore noteworthy that oppositely charged dyes have resulted in similar behaviour, notwithstanding that all membranes were able to achieve, overall, higher levels of MO rejection. It is hypothesised that the greater overall rejection of MO compared to MB was due to a combination of electrostatic repulsive interactions and adsorption of MO by GO coatings through $\pi - \pi$ association. The highest rejection was achieved by the 0.10 mg/mL coating of SFGO, an interesting observation since this material was found to be the poorer adsorbent of MO compared to LFGO. As such, it is suggested that the higher zeta potential and smaller flake sizes were responsible for promoting electrostatic repulsion. Meanwhile, the permeability of MO filtration was lower compared to MB which was considered a further feature of the repulsive forces that counteract permeation. In our previous work on dye-GO interactions [45] we showed that the electronegativity of GO was not significantly impacted by MO, and that GO was found to retain its overall negativity. As such, it was considered that during filtration the membrane continued to provide a negatively charged active layer which barriered the permeation of MO. Given the higher overall rejection of MO, this emphasises the importance of charge and zeta potential in the overall rejection mechanism, thus illustrating the comparison between the two dyes.

3.3. Desalination of saline feeds using GO-coated PES membranes

3.3.1. Impact of filtration pressure

The impact of filtration pressure was investigated by removal of 0.50 g/L salts at pressures of 2 and 4 bar with GO coating concentrations of 0.01 mg/mL and 0.10 mg/mL. The mean permeabilities of the 0.01 mg/mL SFGO membranes are presented in Fig. 6, demonstrating the removal performance for (a) sodium chloride (NaCl), (b) sodium sulphate (Na_2SO_4), (c) magnesium sulphate ($MgSO_4$) and (d) ammonium heptamolybdate ($(NH_4)_6Mo_7O_{24}$) salts. Note that the cation NH_4^+ is used to represent the ammonium salt in the figures below to facilitate viewing. The analogous results for the 0.10 mg/mL SFGO/PES systems are presented in Fig. S8 in the ESM.

Filtering at higher pressure provided the ionic species in the feed with increased energy thus overcoming the inherent resistance to mass transfer from the membrane itself [112]. For the SFGO/PES systems this

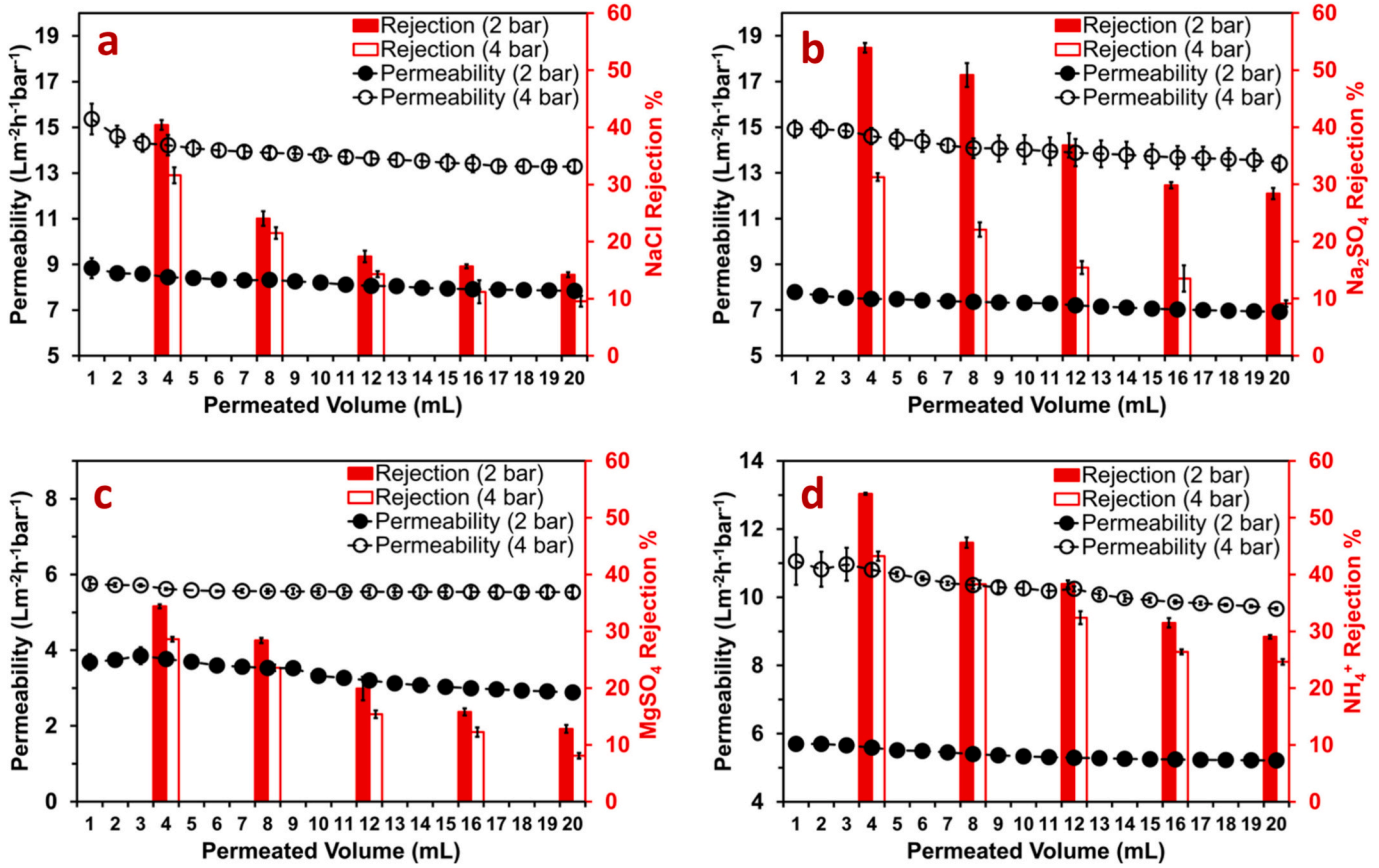

Fig. 6. Permeability and salt rejection as a function of permeated volume in the desalination of (a) sodium chloride, (b) sodium sulphate, (c) magnesium sulphate and (d) ammonium heptamolybdate using a 0.01 mg/mL SFGO coating. The salt concentration was 0.50 g/L and static filtration pressure was 2 and 4 bar. Vertical error bars represent the standard deviation across 3 filtration runs.

resulted in a step increase in filtration pressure results and a corresponding increase in permeability towards all salt solutions, coupled with an associated decline in mean rejection. The trends in permeability and rejection therefore appear to have internal consistency with the results achieved in removal of charged dyes at higher filtration pressure (Section 3.2.3), thus suggesting the associated behaviour with pressure was consistent at 4 bar. Furthermore, permeabilities for the 0.10 mg/mL SFGO coating at 4 bar were consistently lower than the 0.01 mg/mL loadings, whilst overall levels of salt rejection were increased with higher GO concentration. These trends were also consistent with observed behaviour for the SFGO/PES systems at 2 bar. Interestingly, it was found that the rejections of salts decreased over time for all membranes, which may be explained by the fact that the feed concentrations of salts were increased during the test, which led to higher diffusion rate for salt through the membranes. In contrast, the starting feed concentrations of dyes were much lower, so the effects were less apparent.

The mean permeabilities of the 0.01 mg/mL LFGO membranes are shown in Fig. 7, and also demonstrate removal performance for (a) NaCl, (b) Na_2SO_4, (c) $MgSO_4$, and (d) NH_4^+ salts. The 0.10 mg/mL LFGO results are shown in Fig. S9 in the ESM. The LFGO membranes also showed a step increase in permeability, and an associated decline in mean rejection for all salts. The trends in permeability and rejection at 4 bar were consistent with the results obtained at 2 bar in terms of GO coating concentration and with respect to the individual salts. A further explanation of these results will be provided in discussion Section 3.3.3.

For our dye filtration studies we discussed how the presence of mechanical defects was likely to be associated with permeability and rejection characteristics. In desalination experiments, the decline in rejection and increase in permeability was exaggerated due to higher operating pressures. Polymer membranes show a tendency to contract when subjected to high transmembrane pressures and, if the membrane is coated with GO, this may lead to the collapse of internal cavities. The result is that the permeability of membranes tends to decline at higher pressures whilst overall rejection capabilities may increase [113]. One uncertainty is whether the higher filtration pressure of 4 bar was sufficient to collapse membrane cavities. Chong et al. [59] studied the permeation of salts through vacuum-filtered deposition membranes and demonstrated this coating compaction artefact for filtration pressures as high as 10 bar. However, for SFGO and LFGO systems, it was not the case that higher pressure led to lower permeability. We therefore propose the aforementioned mechanical defects were primarily responsible for the behaviour observed in salt systems in addition to dye systems for an increase in filtration pressure from 2 to 4 bar.

3.3.2. *Impact of GO coating concentration*

Mean permeability and salt rejection data for the uncoated PES membrane *i.e.*, representing the case where GO concentration is equal to zero, are presented in Table S4 in the ESM, along with standard deviation errors across three experimental runs. As was consistent with the trends in dye removal experiments, the uncoated polymer exhibited very low mean salt rejection values (<1%, in all cases) and high permeabilities.

The mean permeabilities at a filtration pressure of 2 bar for the SFGO/PES and LFGO/PES systems is shown in Fig. 8a, while mean salt rejections are given in Fig. 8b. To aid clarity the ammonium salt is represented by the cation (NH_4^+).

For the SFGO/PES systems, increasing the GO coating concentration from 0.01 mg/mL to 0.10 mg/mL had the dual effect of reducing permeability whilst improving the levels of salt rejection. Such behaviour was consistent with our MB and MO dye filtration experiments (Section 3.2.2). By analogy to these earlier systems, it was suggested that the increase in mass transfer resistance resulting from higher GO concentration was responsible for this behaviour [114]. For each of the respective salts, at both coating concentrations, mean permeability decreased in the order: P (NaCl) > P (Na_2SO_4) > P (NH_4^+) > P ($MgSO_4$). Meanwhile, rejections decreased according to: R (NH_4^+) > R (Na_2SO_4) >

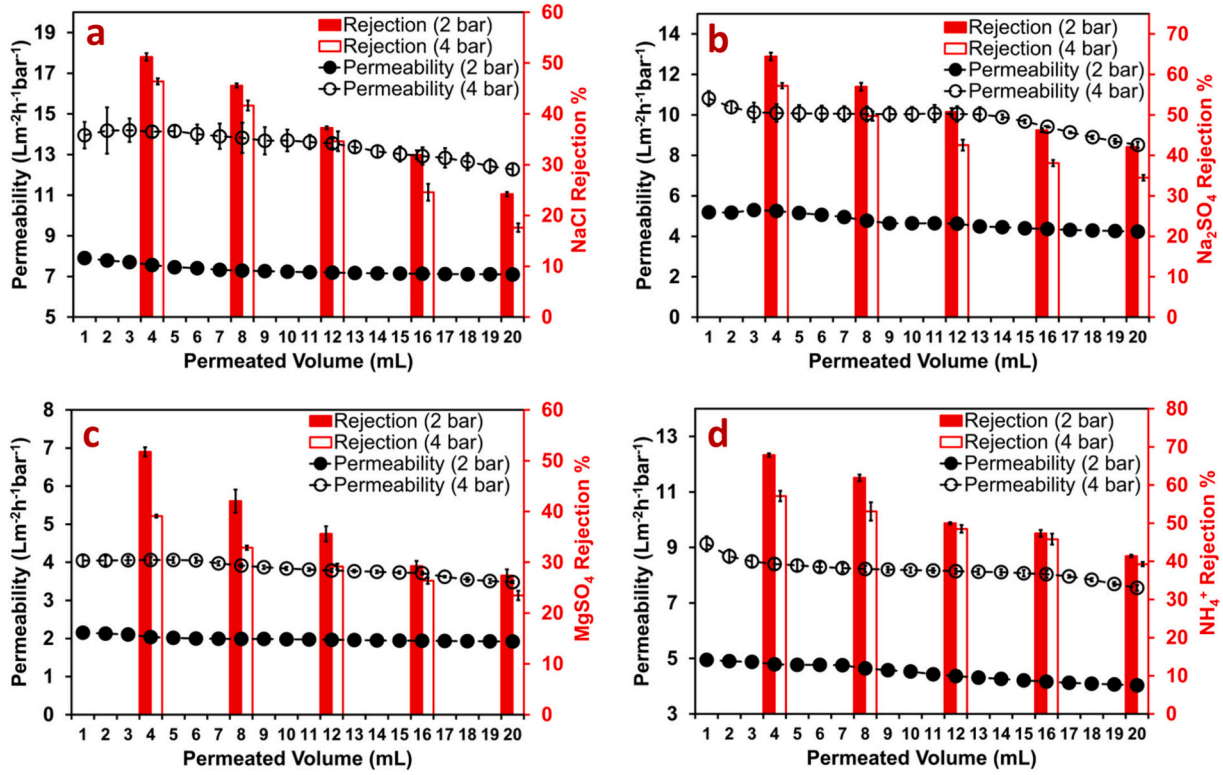

Fig. 7. Permeability and salt rejection as a function of permeated volume in the desalination of (a) sodium chloride, (b) sodium sulphate, (c) magnesium sulphate and (d) ammonium heptamolybdate, using 0.01 mg/mL LFGO coating. The salt concentration was 0.50 g/L and static filtration pressure of 2 or 4 bar. Vertical error bars represent standard deviation across 3 filtration runs.

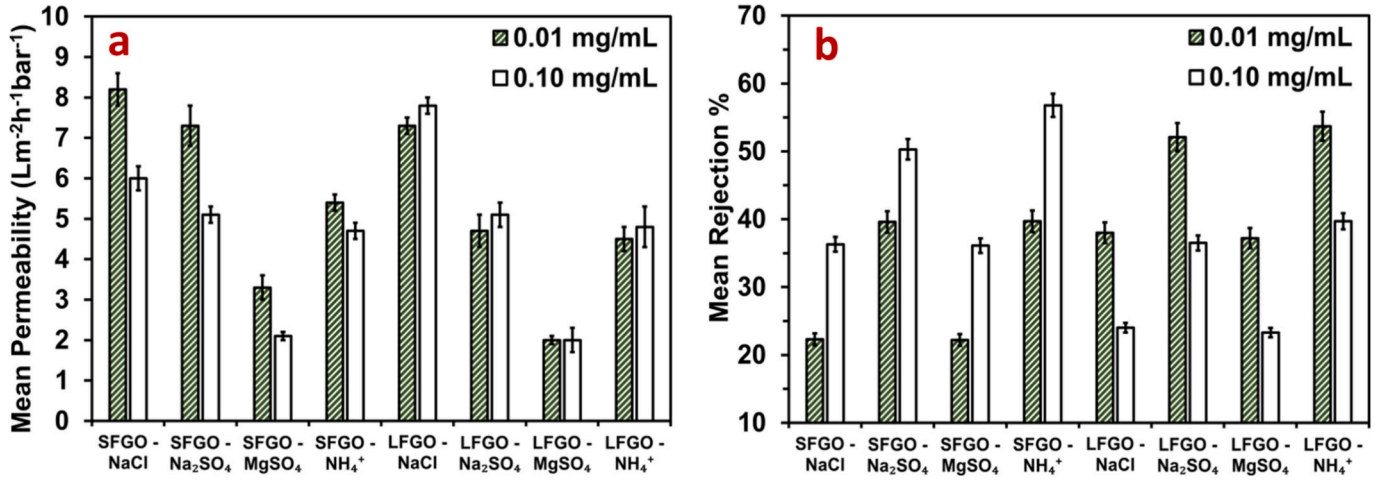

Fig. 8. Impact of GO coating concentration on performance, (a) mean permeability and (b) mean salt rejection of SFGO/PES and LFGO/PES systems measured during dead-end filtration of 0.50 g/L salt solutions. GO coating concentrations were 0.01 and 0.10 mg/mL and static filtration pressure of 2 bar. Vertical error bars represent standard deviation error across three runs.

R (NaCl) ≈ R ($MgSO_4$). We propose that the electrostatic charges of the ionic species were closely associated with the observed experimental trends, though this will be elaborated in the mechanistic discussion (Section 3.3.3).

It was further observed that the permeability of the $MgSO_4$ systems was, in all cases, very low. Divalent cations have higher hydration free energies than monovalent cations and, as such, the energetic barrier associated with their transit is greater [115]. In addition, the electrostatic attraction of the divalent cation to the negatively charged functional groups on the GO is also stronger, thus the cations have potential for intercalation within the GO layers [116,117]. A combination of restrictions and charge resulted in overall lower permeability of cations with higher valency. It was observed that the differences between initial and final permeabilities for 0.01 mg/mL SFGO (Fig. 6) and 0.10 mg/mL SFGO (Fig. S8, in the ESM) exhibited only a very slight decline, suggesting that the effects of concentration polarisation were also minimal, although these systems did not reach equilibrium in these experiments. In this series of experiments, the impact of varying the initial concentration of salt was not studied, although it was proposed that performing experiments with higher salt concentrations may have resulted in a more substantial decline in permeability [113,118]. A further prominent feature was that the rejection of all salts declined as a function of permeated volume, and this characteristic will also be considered in the next section.

For LFGO coatings, the relationship between coating concentration and desalination efficacy was contrary to that of the SFGO coatings. It was found that increasing the GO coating concentration increased the overall mean permeability whilst decreasing mean rejection. These trends in LFGO performance mirror those obtained in our dye removal experiments (Section 3.2.2). With respect to removal of each individual salt, the mean permeability and rejection trends for LFGO was identical to that of the SFGO coatings (as discussed above). In addition, the permeability and rejection profiles as a function of permeated volume followed an analogous trend to the SFGO membranes, given the decline in permeability and rejection as a function of permeated volume (Fig. 7 and S9, in the ESM). These were interesting observations given the starkly different behaviours, subject to changing the coating concentration. Again, this pointed to the dominance of electrostatic charge-based interactions in desalination with GO-coated membranes, and will be addressed later.

3.3.3. *Discussion: Mechanism of desalination*

Electrostatic interactions of ionic species with the electronegative GO coating were considered a salient feature in the desalination mechanism. The Donnan Effect [119,120] is an electrochemical principle driven by discrepancies in charge when dissociated ions present in solution do not distribute evenly across the feed and permeate streams. With respect to GO membranes, anions are termed *co-ions* as they share the negative charge characteristic of the GO, whilst cationic species are termed *counter-ions*. Due to the effects of electrostatic repulsion, the GO surface initially repels co-ions and, as such, their presence is maintained in the feed side [121]. By conservation of electrical charge neutrality on the feed side, counter-ions must also be simultaneously retained [122]. Thus, the greater number of cationic groups per anion leads to higher rejection of ions, as for every permeating anion more cations must transit the membrane in order to maintain overall charge neutrality. The Donnan Effect predicts salt retention is proportional to anionic valency, while having inverse proportionality with cation valence. The respective valence of the cation (Z^+) to the anion (Z^-) may be expressed as a ratio (Z^+/Z^-) which, in accordance with the Donnan Effect, predicts rejection capabilities. Consistent with this hypothesis, a lower Z^+/Z^- therefore leads to higher rejection. The ratios of Z^+/Z^- for the four salts in our systems were: NaCl – 1, $MgSO_4$–1, Na_2SO_4–0.50 and NH_4^+ – 0.167.

In order to examine our systems in relation to the Donnan Effect, the mean salt rejection was plotted as a function of Z^+/Z^- for each of the GO-salt systems considered, see Fig. S10 in the ESM. It appeared the ordering of rejections R (NH_4^+) > R (Na_2SO_4) > R (NaCl) ≈ R ($MgSO_4$) for all systems was therefore consistent with Donnan Effect predictions. The impact of the Donnan Effect was illustrated by two highly interesting comparisons in the salt rejection studies. Firstly, the removal of Na_2SO_4 and $MgSO_4$ as divalent anions was identical, and the significant difference in rejection was attributed to the different valency of the cations. It was clear that the divalent Mg^{2+} cation diminishes rejection to a greater extent than Na^+. The higher charge density of the divalent cation facilitated adsorption onto GO surface groups, in particular bidentate ligand groups such as COO^- therefore causing charge neutralisation of the GO coating [123–125]. The Donnan Effect was weakened by these interactions therefore resulting in lower overall rejection of the Mg^{2+} salt [38]. A second comparison was drawn between $MgSO_4$ and NaCl, both having Z^+/Z^- ratio equal to one. The rejection levels of these salts was very close; in several cases it was marginally higher for NaCl. In terms of anions, the divalent SO_4^{2-} ($-1.147 C/mm^3$) had significantly greater negativity than the monovalent Cl^- ($-0.457 C/mm^3$) [126]. GO membranes, with their initial electronegative coating, therefore repelled SO_4^{2-} more strongly than Cl^-. On the other hand, Mg^{2+} eliminated the electronegativity of the membrane to a greater extent than Na^+, as discussed above. For this comparison of two salts with equal Z^+/Z^-, there was seemingly an interesting relationship between the balance of

attractive and repulsive forces between the GO and counter/co-ionic species, and this had a potent effect on system performance. The effects appeared to reach a state of parity, resulting in very similar levels of rejection overall for these two salts.

GO membranes also separate components based on physical size sieving, an effect known as steric hindrance. In terms of the ions used in our studies the hydrated diameters are: Na^+ (0.72 nm), Mg^{2+} (0.86 nm), NH_4^+ (0.66 nm), Cl^- (0.66 nm) and SO_4^{2-} (0.76 nm) [127]. By measurement of d-spacing using XRD in dry (Fig. 1c) and hydrated state (Fig. S1, in ESM) membranes, it was demonstrated that interlayer spacing of the 0.10 mg/mL coatings for both GO systems in dry state was 0.76 nm. In hydrated state, the SFGO membrane was swollen to 0.80 nm, while LFGO d-spacing increased to 0.82 nm. Based on an argument of steric effects alone it was thus considered the membranes would be unable to retain the small Na^+ and NH_4^+ cations. In practice, however, overall rejection of NH_4^+ salt was highest. Similarly, it was hypothesised that the Cl^- and SO_4^{2-} anions would likewise be capable of permeation. To further illustrate the effects of steric hindrance the removal efficacies of NaCl and Na_2SO_4 were compared. It was found that rejection of sulphate was significantly higher than for chloride; this feature may be attributed to the combined effects of steric hindrance of the larger SO_4^{2-} anion in addition to electrostatic effects [59]. However, considering the above calculated interlayer spacings relative to ionic sizes, it was felt size exclusion was unlikely to be the dominant mechanism of rejection. Steric effects may have contributed to the decline in salt rejection with permeated volume. When the membrane intercalated water molecules, the transport of ions through the swollen structure was facilitated due to the increase in interlayer spacing thus enabling the permeation of a greater number of ions [38].

3.4. Fractionation of dye-salt mixtures using GO-coated PES membranes

Here, the fractionation of binary dye-salt mixtures was considered to explore the impact of varied flake sizes. A number of studies have highlighted the presence of multiple species in the feed stream to have an adverse impact on membrane system performance [128–130]. Textile effluents tend to be complex mixtures of species, including organic dyes and dissolved inorganic salts; for reference a typical effluent composition is provided in Table S5 in the ESM [131–133]. It was therefore important that the GO membranes were tested as a means of fractionating mixed dye-salt systems, since this is an important feature of industrial utility. MB was selected as the target dye, and $MgSO_4$ and Na_2SO_4 as the salts for these studies. Only the two most successful membrane candidates were selected for this series of tests *i.e.*, SFGO/PES 0.10 mg/mL (higher SFGO concentration) and LFGO/PES 0.01 mg/mL (lower LFGO concentration). For brevity, in this section, SFGO/PES 0.10 mg/mL system will be referred to as SFGO, and LFGO/PES 0.01 mg/mL will be shortened to LFGO.

The permeability and dye and salt rejections of the combined dye-salt mixtures is shown in Fig. 9a and b, respectively. The calculated standard deviation error in permeability and respective dye and salt rejections across three experimental runs is provided in Table S6 in the ESM. The permeability and rejection of MB dye in the absence of salt is also included in the plots in order to facilitate comparison between the efficacies of mono-component and binary component feeds.

The presence of ionic species was demonstrated to have an adverse impact on permeability for both membrane systems. The introduction of ions into the MB solution increased the ionic concentration in the feed and, as such, the osmotic pressure increased, and the permeability decreased. This was in line with observations from similar studies [134]. The impact on SFGO membranes was particularly marked; the high MB adsorption capacity and surface area of the SFGO coating promoted cationic adsorption thus accounting for greater depletion in permeability, subject to the increased concentration of feed cations. Furthermore, deposition of dyes onto the membrane surfaces due to adsorption caused a reduction in permeation of solvent in dye-salt systems due to physical pore coverage or blockading [135]. The permeability of both membrane systems towards MB/MgSO4 was lowest overall, likely due to increased adsorption of the divalent cation onto the membrane surface relative to the monovalent Na^+. This may penetrate membrane pores and cause localised shrinkage thus reducing permeability [136].

Comparison of overall mean MB rejections with and without electrolyte revealed MB rejection was decreased subject to ionic presence. The adsorption of cations onto the initially electronegative membrane surface thus had a shielding effect on the negative surface potential [137,138]. In our previous work [45], it was demonstrated that the interaction of cations with solid GO adsorbent surfaces caused a reduction in measured zeta potential. It also revealed that divalent Mg^{2+} cations had the greatest impact on colloidal stability, to the extent that charge reversal was observed at sufficient ionic concentration. This interaction was considered a feature of the greater charge density of Mg^{2+} compared to Na^+. Such behaviour was consistent with the rejection trends observed here as we found the incorporation of magnesium sulphate had greater impact than sodium sulphate on reducing rejection levels of MB.

Furthermore, it has been suggested that the presence of low concentrations of ionic species may actually assist the dispersal of cationic dyes in solution due to repulsive interaction forces between dye

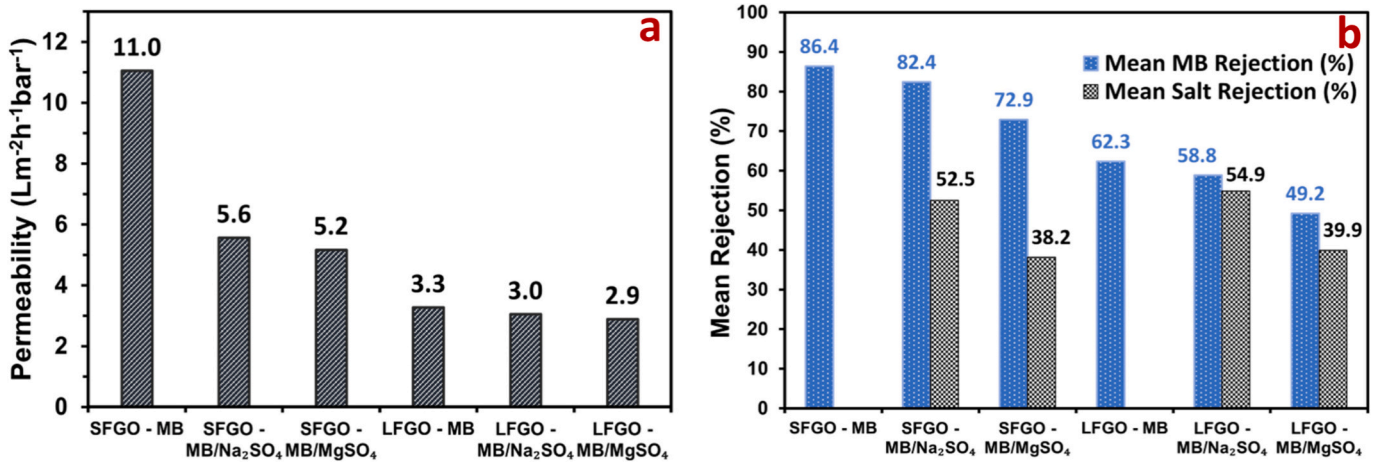

Fig. 9. (a) Mean permeability of SFGO and LFGO systems in fractionation of mixed MB/Na_2SO_4 and MB/$MgSO_4$ mixtures, and (b) combined MB and salt rejection (%) for dye-salt mixtures using SFGO and LFGO systems. On each of the plots the respective results achieved in removal of MB is included for comparison. The filtration pressure was set at 2 bar.

molecules and cations. This drives the dye molecules apart and facilitates dye transit through the membrane [139]. An interesting observation was noted in the recorded levels of salt rejection, as these were found to very slightly increase (relative to the earlier desalination studies) when the salts were dispersed in MB. This observation was considered to be due to the increase in membrane thickness that occurred during deposition of MB onto the electronegative membrane surface; this had the effect of hindering the passage of ions thus slightly increasing the resistance to transport across the membrane [140].

In multi-component feeds, *selectivity* is an important parameter for assessment of separation performance. In fact, achievement of high solvent permeability and high selectivity is a desirable feature in membrane operation [141]. The selectivity parameter (α), provides an assessment of the ability to fractionate different species [142]. Given the salt and dye mixtures in the present study the selectivity of salt separation relative to dye ($\alpha_{(Salt/Dye)}$) was defined by Eq. 4 [143]:

$$\alpha_{(Salt/Dye)} = (1 - R_{Salt})/(1 - R_{Dye}) \quad (4)$$

where R_{Dye} and R_{Salt} are the respective dye and salt rejections.

The calculated values of $\alpha_{(Salt/Dye)}$, including the calculated standard deviational error across three runs, for the SFGO and LFGO systems are reported in Table 1.

It is apparent that the SFGO coating offered improved levels of selectivity compared to the LFGO for both dye-salt combinations. This was considered a feature of the SFGO coatings retaining high overall levels of MB rejection thus maximising the values of $\alpha_{(Salt/Dye)}$. For the current systems, the calculated values of $\alpha_{(Salt/Dye)}$ were all relatively low in comparison to composite GO material coatings reported elsewhere. For example, Kang et al. [143] reported a highly selective magnetite-doped GO membrane that achieved a selectivity of 63.2 when filtering a Congo Red/NaCl system. Similarly, Li et al. [144] reported a selective trimethylamine-doped membrane that achieved a selectivity of 18.3 when separating a Congo Red/Na_2SO_4 system. It is thus considered that the selectivity of membrane systems may be improved by functionalisation of the GO to tailor its properties towards rejection of a particular component.

Table 1
Calculated values of $\alpha_{(Salt/Dye)}$, including standard deviation error, for selective separation of MB/$MgSO_4$ and MB/Na_2SO_4 mixtures.

GO coating	Dye-salt mixture	$\alpha_{(Salt/Dye)}$	Error in $\alpha_{(Salt/Dye)}$
SFGO	MB/Na_2SO_4	2.7	0.040
	MB/$MgSO_4$	2.3	0.015
LFGO	MB/Na_2SO_4	1.1	0.007
	MB/$MgSO_4$	1.2	0.012

4. Conclusions

In this study, the structure-property relationships governing the performance of GO membranes in remediation of dye and salt-contaminated wastewaters were systematically investigated. Due to its simplicity and ability to produce uniform coatings, vacuum filtration was used to fabricate GO-coated PES membranes. In dye removal studies, membranes were effective in removal of both cationic MB and anionic MO. In particular, the 0.10 mg/mL dispersion coating of SFGO was shown to be most effective in removal of both dyes due to its highly negative zeta potential, high surface area and small flake size, resulting in high permeabilities alongside promising dye rejection capabilities. Interestingly, in LFGO systems, the higher concentration 0.10 mg/mL dispersion coating was less effective compared to its 0.01 mg/mL counterpart, owing to partial coating delamination after immersion, highlighting the significance of flake size. Mechanistically, separation of both dyes is driven by a combination of factors including adsorption, electrostatic interactions and size-based exclusion.

GO-coated membranes were also demonstrated to have reasonable capacity to desalinate salt solutions, with salt rejection decreasing according to $R\ (NH_4^+) > R\ (Na_2SO_4) > R\ (NaCl) \approx R\ (MgSO_4)$. Salt rejection by GO-coated membranes was largely attributed to the Donnan Effect, as the highest overall rejections were achieved by salts having the lowest cationic valency and highest anionic valency *i.e.,* ammonium heptamolybdate and sodium sulphate).

From a practical perspective, this study provides a systematic exploration of structure-property relationships linking GO flake size with membrane physicochemical characteristics and separation performance. The findings offer valuable insight for design of composite membrane systems targeting industrial wastewater treatment, offering guidance on material selection and screening, membrane fabrication and performance optimisation. Furthermore, it is expected that the results will assist efforts to expand the utility of GO membranes, including through chemical functionalisation, for which the role of flake size is anticipated to be highly significant.

CRediT authorship contribution statement

James M. Exley: Writing – original draft, Validation, Methodology, Investigation, Formal analysis, Data curation, Conceptualization. **Timothy N. Hunter:** Writing – review & editing, Supervision, Methodology, Conceptualization. **Fan Fei:** Writing – review & editing, Supervision, Methodology, Conceptualization. **Thomas Pugh:** Writing – review & editing, Supervision, Methodology, Conceptualization. **Martin R. Tillotson:** Writing – review & editing, Supervision, Project administration, Methodology, Conceptualization.

Declaration of competing interest

The authors declare the following financial interests/personal relationships which may be considered as potential competing interests: James Exley reports financial support was provided by UK Research and Innovation. James Exley reports financial support was provided by Engineering and Physical Sciences Research Council. James Exley reports financial support was provided by Evove Limited. If there are other authors, they declare that they have no known competing financial interests or personal relationships that could have appeared to influence the work reported in this paper.

Acknowledgements

This study was supported by funding through a doctoral award from Engineering and Physical Sciences Research Council (EPSRC) UK (grant reference EP/M50807X/1) and Evove Limited (grant reference EP/R513258/1). The authors are grateful to the funders and acknowledge their support of this work.

The authors would like to express gratitude to the following, based in University of Leeds, who have provided technical support and/or training: Dr. Ben Douglas (water contact angle), Ms. Lucy Leonard (FTIR, TGA), Dr. Faye Esat (XRD), Mr. Stuart Mickelthwaite (FIBSEM). In addition, Ms. Karen Stevens, Dr. David Elliott, Mr. Morgan McGowan and Ms. Emma Tidswell have provided technical support and training in relation to filtration studies, including safe setup and operation of the Sterlitech HP4750 equipment.

Appendix A. Supplementary data

Supplementary data to this article can be found online at https://doi.org/10.1016/j.flatc.2026.101017.

Data availability

Data will be made available on request.

References

[1] X. Du, et al., A review on the mechanism, impacts and control methods of membrane fouling in MBR system, Membranes 10 (2) (2020) 24.
[2] Q. She, et al., Membrane fouling in osmotically driven membrane processes: a review, J. Membr. Sci. 499 (2016) 201–233.
[3] H. Abdelrazeq, et al., Sustainable innovation in membrane technologies for produced water treatment: challenges and limitations, Sustainability 13 (12) (2021) 6759.
[4] N. Voutchkov, Energy use for membrane seawater desalination–current status and trends, Desalination 431 (2018) 2–14.
[5] M. Elimelech, W.A. Phillip, The future of seawater desalination: energy, technology, and the environment, science 333 (6043) (2011) 712–717.
[6] D. Janowitz, et al., Can large-scale offshore membrane desalination cost-effectively and ecologically address water scarcity in the Middle East? Membranes 12 (3) (2022) 323.
[7] K. Krishnamoorthy, M. Veerapandian, K. Yun, S.-J. Kim, The chemical and structural analysis of graphene oxide with different degrees of oxidation, Carbon 53 (2013) 38–49.
[8] R.K. Joshi, et al., Graphene oxide: the new membrane material, Appl. Mater. Today 1 (1) (2015) 1–12.
[9] K. Huang, et al., A graphene oxide membrane with highly selective molecular separation of aqueous organic solution, Angew. Chem. 126 (27) (2014) 7049–7052.
[10] M. Zhang, et al., Controllable ion transport by surface-charged graphene oxide membrane, Nat. Commun. 10 (1) (2019) 1253.
[11] W. Zhang, et al., Fast and considerable adsorption of methylene blue dye onto graphene oxide, Bull. Environ. Contam. Toxicol. 87 (1) (2011) 86.
[12] G.K. Ramesha, et al., Graphene and graphene oxide as effective adsorbents toward anionic and cationic dyes, J. Colloid Interface Sci. 361 (1) (2011) 270–277.
[13] D. Robati, et al., Removal of hazardous dyes-BR 12 and methyl orange using graphene oxide as an adsorbent from aqueous phase, Chem. Eng. J. 284 (2016) 687–697.
[14] J. Deng, et al., Mechanism of water transport in graphene oxide laminates, Chem. Sci. 8 (3) (2017) 1701–1704.
[15] O. Kwon, et al., Fabrication techniques for graphene oxide-based molecular separation membranes: towards industrial application, Nanomaterials 11 (3) (2021) 757.
[16] D. Li, et al., Processable aqueous dispersions of graphene nanosheets, Nat. Nanotechnol. 3 (2) (2008) 101–105.
[17] J. Lyu, et al., Separation and purification using GO and r-GO membranes, RSC Adv. 8 (41) (2018) 23130–23151.
[18] G. Eda, G. Fanchini, M. Chhowalla, Large-area ultrathin films of reduced graphene oxide as a transparent and flexible electronic material, Nat. Nanotechnol. 3 (5) (2008) 270–274.
[19] D.A. Dikin, et al., Preparation and characterization of graphene oxide paper, Nature 448 (7152) (2007) 457–460.
[20] Y. Wei, et al., Multilayered graphene oxide membranes for water treatment: a review, Carbon 139 (2018) 964–981.
[21] N.A. Elessawy, et al., Development of an efficient, low-operating-pressure graphene oxide/polyethersulfone nanofiltration membrane for removing various water contaminants, J. Environ. Chem. Eng. 12 (2) (2024) 112489.
[22] M. Mahmoudian, M.G. Kochameshki, The performance of polyethersulfone nanocomposite membrane in the removal of industrial dyes, Polymer 224 (2021) 123693.
[23] M. Zambianchi, et al., Graphene oxide-polysulfone hollow fibers membranes with synergic ultrafiltration and adsorption for enhanced drinking water treatment, J. Membr. Sci. 658 (2022) 120707.
[24] X. Wang, et al., Fabrication of graphene oxide/polydopamine adsorptive membrane by stepwise in-situ growth for removal of rhodamine B from water, Desalination 516 (2021) 115220.
[25] C.R. Minitha, et al., Adsorption behaviour of reduced graphene oxide towards cationic and anionic dyes: co-action of electrostatic and π – π interactions, Mater. Chem. Phys. 194 (2017) 243–252.
[26] Y. Song, et al., Efficient removal and fouling-resistant of anionic dyes by nanofiltration membrane with phosphorylated chitosan modified graphene oxide nanosheets incorporated selective layer, J. Water Process Eng. 34 (2020) 101086.
[27] E.F.D. Januário, et al., Advanced graphene oxide-based membranes as a potential alternative for dyes removal: a review, Sci. Total Environ. 789 (2021) 147957.
[28] Y. You, et al., Graphene and graphene oxide for desalination, Nanoscale 8 (1) (2016) 117–119.
[29] H.M. Hegab, L. Zou, Graphene oxide-assisted membranes: fabrication and potential applications in desalination and water purification, J. Membr. Sci. 484 (2015) 95–106.
[30] D.J. Johnson, N. Hilal, Can graphene and graphene oxide materials revolutionise desalination processes? Desalination 500 (2021) 114852.
[31] R. Ge, et al., GO-based membranes for desalination, Membranes 13 (2) (2023) 220.
[32] A. Boretti, et al., Outlook for graphene-based desalination membranes, Npj clean Water 1 (1) (2018) 5.
[33] Z. Wang, et al., The stability of a graphene oxide (GO) nanofiltration (NF) membrane in an aqueous environment: Progress and challenges, Materials Advances 1 (4) (2020) 554–568.
[34] R. Liu, et al., Graphene oxide membrane for liquid phase organic molecular separation, Carbon 77 (2014) 933–938.
[35] Z. Jia, et al., Diamines cross-linked graphene oxide free-standing membranes for ion dialysis separation, J. Membr. Sci. 520 (2016) 139–144.
[36] S. Zheng, et al., Swelling of graphene oxide membranes in aqueous solution: characterization of interlayer spacing and insight into water transport mechanisms, ACS Nano 11 (6) (2017) 6440–6450.
[37] Y. Mo, X. Zhao, Y.-X. Shen, Cation-dependent structural instability of graphene oxide membranes and its effect on membrane separation performance, Desalination 399 (2016) 40–46.
[38] R. Hu, et al., The application feasibility of graphene oxide membranes for pressure-driven desalination in a dead-end flow system, Desalination 477 (2020) 114271.
[39] L. Zhang, et al., Effect of physical and chemical structures of graphene oxide on water permeation in graphene oxide membranes, Appl. Surf. Sci. 520 (2020) 146308.
[40] J. Chong, B. Wang, K. Li, Graphene oxide membranes in fluid separations, Curr. Opin. Chem. Eng. 12 (2016) 98–105.
[41] L. Nie, et al., Realizing small-flake graphene oxide membranes for ultrafast size-dependent organic solvent nanofiltration, Sci. Adv. 6 (17) (2020) eaaz9184.
[42] N. Akther, et al., Influence of graphene oxide lateral size on the properties and performances of forward osmosis membrane, Desalination 484 (2020) 114421.
[43] X. Ai, et al., Graphene oxide membranes with hierarchical structures used for molecule sieving, Sep. Purif. Technol. 230 (2020) 115879.
[44] P. Sun, et al., Selective trans-membrane transport of alkali and alkaline earth cations through graphene oxide membranes based on cation− π interactions, ACS Nano 8 (1) (2014) 850–859.
[45] J.M. Exley, et al., Influence of flake size and electrolyte conditions on graphene oxide adsorption of ionic dyes, Powder Technol. (2023) 118387.
[46] Y. Li, T. Zhao, W. Yang, Measurements of water uptake and transport properties in anion-exchange membranes, Int. J. Hydrogen Energy 35 (11) (2010) 5656–5665.
[47] W.H. Bragg, W.L. Bragg, *The reflection of X-rays by crystals.* Proceedings of the Royal Society of London, Series A, Containing Papers of a Mathematical and Physical Character 88 (605) (1913) 428–438.
[48] H. Jee, et al., Enhancing the dye-rejection efficiencies and stability of graphene oxide-based nanofiltration membranes via divalent cation intercalation and mild reduction, Membranes 12 (4) (2022) 402.
[49] C. Quezada, et al., Prediction of permeate flux in ultrafiltration processes: a review of modeling approaches, Membranes 11 (5) (2021) 368.
[50] T. Teorell, An attempt to formulate a quantitative theory of membrane permeability, Proc. Soc. Exp. Biol. Med. 33 (2) (1935) 282–285.
[51] R. Yi, et al., Ultrahigh permeance of a chemical cross-linked graphene oxide nanofiltration membrane enhanced by cation–π interaction, RSC Adv. 9 (69) (2019) 40397–40403.
[52] K. Noel Jacob, et al., Sulfonated polyethersulfone-based membranes for metal ion removal via a hybrid process, J. Mater. Sci. 49 (1) (2014) 114–122.
[53] A.K. Ali, et al., Proton exchange membrane based on graphene oxide/polysulfone hybrid nano-composite for simultaneous generation of electricity and wastewater treatment, J. Hazard. Mater. 419 (2021) 126420.
[54] K. Zahri, et al., Graphene oxide/polysulfone hollow fiber mixed matrix membranes for gas separation, RSC Adv. 6 (92) (2016) 89130–89139.
[55] T. Forati, et al., Physical and mechanical properties of graphene oxide/polyethersulfone nanocomposites, Polym. Adv. Technol. 25 (3) (2014) 322–328.
[56] J. Wang, H. Jiang, N. Jiang, Study on the pyrolysis of phenol-formaldehyde (PF) resin and modified PF resin, Thermochim. Acta 496 (1–2) (2009) 136–142.
[57] M. Ionita, et al., Improving the thermal and mechanical properties of polysulfone by incorporation of graphene oxide, Compos. Part B Eng. 59 (2014) 133–139.
[58] J. Alam, et al., Graphene oxide, an effective nanoadditive for a development of hollow fiber nanocomposite membrane with antifouling properties, Adv. Polym. Technol. 37 (7) (2018) 2597–2608.
[59] J.Y. Chong, et al., Dynamic microstructure of graphene oxide membranes and the permeation flux, J. Membr. Sci. 549 (2018) 385–392.
[60] C. Peng, et al., Graphene oxide-based membrane as a protective barrier against toxic vapors and gases, ACS Appl. Mater. Interfaces 12 (9) (2020) 11094–11103.
[61] L. Badrinezhad, et al., Preparation and characterization of polysulfone/graphene oxide nanocomposite membranes for the separation of methylene blue from water, Polym. Bull. 75 (2) (2018) 469–484.
[62] M. Sabet, H. Soleimani, Influence of graphene oxide on the mechanical, thermal and roughness of polyethersulphone, Bull. Mater. Sci. 45 (1) (2022) 1–12.
[63] C. Luo, et al., A cut-and-paste approach to 3D graphene-oxide-based architectures, Adv. Mater. 30 (15) (2018) 1706229.
[64] N. Giovambattista, P.G. Debenedetti, P.J. Rossky, Effect of surface polarity on water contact angle and interfacial hydration structure, J. Phys. Chem. B. 111 (32) (2007) 9581–9587.
[65] A. Marjani, et al., Effect of graphene oxide on modifying polyethersulfone membrane performance and its application in wastewater treatment, Sci. Rep. 10 (1) (2020) 1–11.
[66] O.Z. Higa, L.M. Sakuno, A.A. de Queiroz, Dendrimer Functionalized Radiation Grafted Hydrogels for Tissue Engineering Applications, 2009.
[67] R. Joshi, et al., Precise and ultrafast molecular sieving through graphene oxide membranes, Science 343 (6172) (2014) 752–754.
[68] K.W. Putz, et al., Evolution of order during vacuum-assisted self-assembly of graphene oxide paper and associated polymer nanocomposites, ACS Nano 5 (8) (2011) 6601–6609.
[69] P. Banerjee, A. Mukhopadhyay, P. Das, Graphene oxide–nanobentonite composite sieves for enhanced desalination and dye removal, Desalination 451 (2019) 231–240.

[70] I. Taniguchi, et al., A compatible crosslinker for enhancement of CO2 capture of poly (amidoamine) dendrimer-containing polymeric membranes, J. Membr. Sci. 475 (2015) 175–183.
[71] H. Hernandez-Martinez, et al., Mixed matrix membranes based on fluoropolymers with m-and p-terphenyl fragments for gas separation applications, ACS Omega 6 (7) (2021) 4921–4931.
[72] Z. Zhang, et al., Influence of particle concentration on the elemental penetration region and properties of Ni-P-SiC composite coatings prepared through sandblasting and scanning electrodeposition on 45 steel surfaces, Coatings 11 (10) (2021) 1237.
[73] S. Gorgieva, R. Vogrinčič, V. Kokol, The effect of membrane structure prepared from carboxymethyl cellulose and cellulose nanofibrils for cationic dye removal, J. Polym. Environ. 27 (2) (2019) 318–332.
[74] L. Shao, et al., Newly developed nanofiltration (NF) composite membranes by interfacial polymerization for safranin O and aniline blue removal, J. Membr. Sci. 430 (2013) 96–105.
[75] A.E. Abdelhamid, A.A. El-Sayed, A.M. Khalil, Polysulfone nanofiltration membranes enriched with functionalized graphene oxide for dye removal from wastewater, J. Polym. Eng. 40 (10) (2020) 833–841.
[76] J. Huang, K. Zhang, The high flux poly (m-phenylene isophthalamide) nanofiltration membrane for dye purification and desalination, Desalination 282 (2011) 19–26.
[77] Y. Gao, et al., A metal-nano GO frameworks/PPS membrane with super water flux and high dyes interception, J. Membr. Sci. 574 (2019) 55–64.
[78] Q. Yang, et al., Ultrathin graphene-based membrane with precise molecular sieving and ultrafast solvent permeation, Nat. Mater. 16 (12) (2017) 1198–1202.
[79] C.A. Ruiz-Torres, et al., Graphene-based ultrafast nanofiltration membrane under cross-flow operation: effect of high-flux and filtered solute on membrane performance, Carbon 185 (2021) 641–649.
[80] X. Kang, et al., Bio-inspired co-deposited preparation of GO composite loose nanofiltration membrane for dye contaminated wastewater sustainable treatment, J. Hazard. Mater. 400 (2020) 123121.
[81] F. Jia, et al., Efficient separation of dyes using two-dimensional heterogeneous composite membranes, Water Res. 247 (2023) 120693.
[82] J.G. Wijmans, R.W. Baker, The solution-diffusion model: a review, J. Membr. Sci. 107 (1–2) (1995) 1–21.
[83] J. Fralliccardi, et al., Membrane thickness, lipid phase and sterol type are determining factors in the permeability of membranes to small solutes, Nat. Commun. 13 (1) (2022) 1–12.
[84] B.J. Zwolinski, H. Eyring, C.E. Reese, Diffusion and membrane permeability, J. Phys. Chem. 53 (9) (1949) 1426–1453.
[85] N.C. Homem, et al., Surface modification of a polyethersulfone microfiltration membrane with graphene oxide for reactive dyes removal, Appl. Surf. Sci. 486 (2019) 499–507.
[86] J. Zhang, et al., Improved hydrophilicity, permeability, antifouling and mechanical performance of PVDF composite ultrafiltration membranes tailored by oxidized low-dimensional carbon nanomaterials, J. Mater. Chem. A 1 (9) (2013) 3101–3111.
[87] A. Ahmad, et al., Recent development in additives modifications of polyethersulfone membrane for flux enhancement, Chem. Eng. J. 223 (2013) 246–267.
[88] K. Nandy, et al., Stop motion animation reveals formation mechanism of hierarchical structure in graphene oxide papers, Adv. Mater. Interfaces 3 (6) (2016) 1500666.
[89] C.-H. Tsou, et al., Effect of microstructure of graphene oxide fabricated through different self-assembly techniques on 1-butanol dehydration, J. Membr. Sci. 477 (2015) 93–100.
[90] P. Su, et al., Graphene oxide membranes: controlling their transport pathways, J. Mater. Chem. A 8 (31) (2020) 15319–15340.
[91] A. Gogoi, A. Koneru, K.A. Reddy, Effect of graphene oxide (GO) nanosheet sizes, pinhole defects and non-ideal lamellar stacking on the performance of layered GO membranes: an atomistic investigation, Nanoscale Advances 1 (8) (2019) 3023–3035.
[92] J. Li, et al., Improved water permeability and structural stability in a polysulfone-grafted graphene oxide composite membrane used for dye separation, J. Membr. Sci. 595 (2020) 117547.
[93] J.H. Kim, et al., Scalable fabrication of deoxygenated graphene oxide nanofiltration membrane by continuous slot-die coating, J. Membr. Sci. 612 (2020) 118454.
[94] W. Wu, et al., Recent development of graphene oxide based forward osmosis membrane for water treatment: a critical review, Desalination 491 (2020) 114452.
[95] L.Y. Ng, H.S. Chua, C.Y. Ng, Incorporation of graphene oxide-based nanocomposite in the polymeric membrane for water and wastewater treatment: a review on recent development, J. Environ. Chem. Eng. 9 (5) (2021) 105994.
[96] M. Hu, S. Zheng, B. Mi, Organic fouling of graphene oxide membranes and its implications for membrane fouling control in engineered osmosis, Environ. Sci. Technol. 50 (2) (2016) 685–693.
[97] W. Guo, H.-H. Ngo, J. Li, A mini-review on membrane fouling, Bioresour. Technol. 122 (2012) 27–34.
[98] R. Mukherjee, P. Bhunia, S. De, Impact of graphene oxide on removal of heavy metals using mixed matrix membrane, Chem. Eng. J. 292 (2016) 284–297.
[99] T. Subrahmanya, et al., An eco-friendly and reusable syringe filter membrane for the efficient removal of dyes from water via low pressure filtration assisted self-assembling of graphene oxide and SBA-15/PDA, J. Clean. Prod. 349 (2022) 131425.
[100] V. Kandjou, et al., Enhanced covalent p-phenylenediamine crosslinked graphene oxide membranes: towards superior contaminant removal from wastewaters and improved membrane reusability, J. Hazard. Mater. 380 (2019) 120840.
[101] X. Yan, et al., Layer-by-layer assembly of bio-inspired borate/graphene oxide membranes for dye removal, Chemosphere 256 (2020) 127118.
[102] X. Fan, et al., Hydrothermal reduced graphene oxide membranes for dyes removing, Sep. Purif. Technol. 241 (2020) 116730.
[103] H. Ahmad, et al., Preparation of polyvinylidene fluoride nano-filtration membranes modified with functionalized graphene oxide for textile dye removal, Membranes 12 (2) (2022) 224.
[104] A.B. Fradj, et al., Removal of azoic dyes from aqueous solutions by chitosan enhanced ultrafiltration, Results Chem. 2 (2020) 100017.
[105] Y. Wang, et al., Novel ag-AgBr decorated composite membrane for dye rejection and photodegradation under visible light, Front. Chem. Sci. Eng. 15 (2021) 892–901.
[106] A.J. Kajekar, et al., Preparation and characterization of novel PSf/PVP/PANI-nanofiber nanocomposite hollow fiber ultrafiltration membranes and their possible applications for hazardous dye rejection, Desalination 365 (2015) 117–125.
[107] G. Liu, et al., Graphene oxide for high-efficiency separation membranes: role of electrostatic interactions, Carbon 110 (2016) 56–61.
[108] P. Zhang, et al., Improving stability and separation performance of graphene oxide/graphene nanofiltration membranes by adjusting the laminated regularity of stacking-sheets, Sci. Total Environ. 827 (2022) 154175.
[109] M.F. Abid, M.A. Zablouk, A.M. Abid-Alameer, Experimental study of dye removal from industrial wastewater by membrane technologies of reverse osmosis and nanofiltration, Iranian journal of environmental health science & engineering 9 (1) (2012) 1–9.
[110] S. Zinadini, et al., Preparation of a novel antifouling mixed matrix PES membrane by embedding graphene oxide nanoplates, J. Membr. Sci. 453 (2014) 292–301.
[111] H. Wang, et al., Graphene oxide edge grafting of polyaniline nanocomposite: an efficient adsorbent for methylene blue and methyl orange, Water Sci. Technol. 77 (12) (2018) 2751–2760.
[112] H. Dai, Z. Xu, X. Yang, Water permeation and ion rejection in layer-by-layer stacked graphene oxide nanochannels: a molecular dynamics simulation, J. Phys. Chem. C 120 (39) (2016) 22585–22596.
[113] H. Huang, et al., Salt concentration, pH and pressure controlled separation of small molecules through lamellar graphene oxide membranes, Chem. Commun. 49 (53) (2013) 5963–5965.
[114] B. Liang, et al., High performance graphene oxide/polyacrylonitrile composite pervaporation membranes for desalination applications, J. Mater. Chem. A 3 (9) (2015) 5140–5147.
[115] B. Tansel, Significance of thermodynamic and physical characteristics on permeation of ions during membrane separation: hydrated radius, hydration free energy and viscous effects, Sep. Purif. Technol. 86 (2012) 119–126.
[116] P. Sun, et al., Selective ion penetration of graphene oxide membranes, ACS Nano 7 (1) (2013) 428–437.
[117] A. Ghaffar, et al., Scalable graphene oxide membranes with tunable water channels and stability for ion rejection, Environ. Sci. Nano 6 (3) (2019) 904–915.
[118] Y. Han, Z. Xu, C. Gao, Ultrathin graphene nanofiltration membrane for water purification, Adv. Funct. Mater. 23 (29) (2013) 3693–3700.
[119] F.G. Donnan, The theory of membrane equilibria, Chem. Rev. 1 (1) (1924) 73–90.
[120] F.G. Donnan, Theorie der Membrangleichgewichte und Membranpotentiale bei Vorhandensein von nicht dialysierenden Elektrolyten. Ein Beitrag zur physikalisch-chemischen Physiologie, Zeitschrift für Elektrochemie und angewandte physikalische Chemie 17 (14) (1911) 572–581.
[121] R. Epsztein, et al., Role of ionic charge density in donnan exclusion of monovalent anions by nanofiltration, Environ. Sci. Technol. 52 (7) (2018) 4108–4116.
[122] Lejarazu-Larrañaga, A., et al., Nitrate removal by Donnan dialysis and anion-exchange membrane bioreactor using upcycled end-of-life reverse osmosis membranes. Membranes, 2022. 12(2): p. 101.
[123] M. Wang, et al., The dispersion and aggregation of graphene oxide in aqueous media, Nanoscale 8 (30) (2016) 14587–14592.
[124] F. Baskoro, et al., Graphene oxide-cation interaction: inter-layer spacing and zeta potential changes in response to various salt solutions, J. Membr. Sci. 554 (2018) 253–263.
[125] A. Doi, et al., Specificity and affinity of multivalent ions adsorption to kaolinite surface, Appl. Clay Sci. 190 (2020) 105557.
[126] R. Mukherjee, P. Bhunia, S. De, Nanofiltration range desalination by high flux graphene oxide impregnated ultrafiltration hollow fiber mixed matrix membrane, J. Clean. Prod. 213 (2019) 393–405.
[127] E. Guertal, J. Hattey, A scale model of cation exchange for classroom demonstration, Journal of Natural Resources and Life Sciences Education 25 (2) (1996) 125–127.
[128] A. Akbari, et al., Application of nanofiltration hollow fibre membranes, developed by photografting, to treatment of anionic dye solutions, J. Membr. Sci. 297 (1–2) (2007) 243–252.
[129] Y. Zheng, et al., Positively charged thin-film composite hollow fiber nanofiltration membrane for the removal of cationic dyes through submerged filtration, Desalination 328 (2013) 42–50.
[130] G. Syed Ibrahim, et al., One-step synthesis of zwitterionic graphene oxide nanohybrid: application to polysulfone tight ultrafiltration hollow fiber membrane, Sci. Rep. 10 (1) (2020) 1–13.
[131] R.F. Dos Santos, et al., Influence of different textile fibers on characterization of dyeing wastewater and final effluent, Environ. Monit. Assess. 190 (2018) 1–12.

[132] P. Pal, Industrial Water Treatment Process Technology, Butterworth-Heinemann, 2017.
[133] C. Thamaraiselvan, M. Noel, Membrane processes for dye wastewater treatment: recent progress in fouling control, Crit. Rev. Environ. Sci. Technol. 45 (10) (2015) 1007–1040.
[134] L. Liu, et al., Functionalized graphene oxide modified polyethersulfone membranes for low-pressure anionic dye/salt fractionation, Polymers 10 (7) (2018) 795.
[135] P. Chen, et al., Performance of ceramic nanofiltration membrane for desalination of dye solutions containing NaCl and Na2SO4, Desalination 404 (2017) 102–111.
[136] E. Alventosa-deLara, et al., Ultrafiltration ceramic membrane performance during the treatment of model solutions containing dye and salt, Sep. Purif. Technol. 129 (2014) 96–105.
[137] C.Y. Tang, T. Chong, A.G. Fane, Colloidal interactions and fouling of NF and RO membranes: a review, Adv. Colloid Interface Sci. 164 (1–2) (2011) 126–143.
[138] N. Mehrabi, H. Lin, N. Aich, Deep eutectic solvent functionalized graphene oxide nanofiltration membranes with superior water permeance and dye desalination performance, Chem. Eng. J. 412 (2021) 128577.
[139] L. Wang, et al., Covalent crosslinked assembly of tubular ceramic-based multilayer nanofiltration membranes for dye desalination, AIChE J. 59 (10) (2013) 3834–3842.
[140] J. Hu, et al., Polymer brush-modified graphene oxide membrane with excellent structural stability for effective fractionation of textile wastewater, J. Membr. Sci. 618 (2021) 118698.
[141] H.B. Park, et al., Maximizing the right stuff: the trade-off between membrane permeability and selectivity, Science 356 (6343) (2017) eaab0530.
[142] B.D. Freeman, Basis of permeability/selectivity tradeoff relations in polymeric gas separation membranes, Macromolecules 32 (2) (1999) 375–380.
[143] Y. Kang, et al., Dye adsorptive thin-film composite membrane with magnetite decorated sulfonated graphene oxide for efficient dye/salt mixture separation, Desalination 524 (2022) 115462.
[144] M. Li, et al., Graphene oxide nanofiltration membrane with trimethylamine-N-oxide zwitterions for robust biofouling resistance, J. Membr. Sci. 640 (2021) 119855.